CHAPTER III

THE EXPERIMENTAL SET UP AND DATA ANALYSIS

The present experiment, whose results are being reported in this thesis, was a part of the on-going investigation of electron and muon components of Cosmic Ray extensive air shower (EAS) being performed with the NBU air shower array. The array, described previously also by other authors [1-3], has separate units working in conjunction with each other for the detection and measurement of electron and muon components of EAS of sizes in the range of about 10^4 to 10^6 particles at near sea level (~1000 gm/cm^2). At present, few changes have been made to the array with the inclusion of fast timing detectors for determining the arrival direction of the showers. But, when the present experiment was performed the array was operated with 21 scintillation counters in conjunction with two shielded magnetic spectrographs. The design, construction and the characteristics of the different units of the array, which were in use at the time of performance of the present experiment, are described in the Section-I of this chapter. The details of method of data analysis for both electron and muon components along with the estimation of errors in determining the shower parameters from the electron density measurements and those involved in calculating the momenta of muons are described in the Section-II of this chapter.

SECTION-1

THE EXPERIMENTAL SET UP

3.1 THE AIR SHOWER ARRAY

The NBU air shower array, as mentioned earlier, consists of two different units working in conjunction with each other for the study of electrons and muons of the EAS. During the performance of the present experiment, 21 scintillation counters spreading over an area of about 1200m^2 were used for the measurement of electron densities at different points of the incident shower front. The scintillation counters were of two different sizes- 0.250 m^2 and 0.125 m^2 and were arranged in such a way

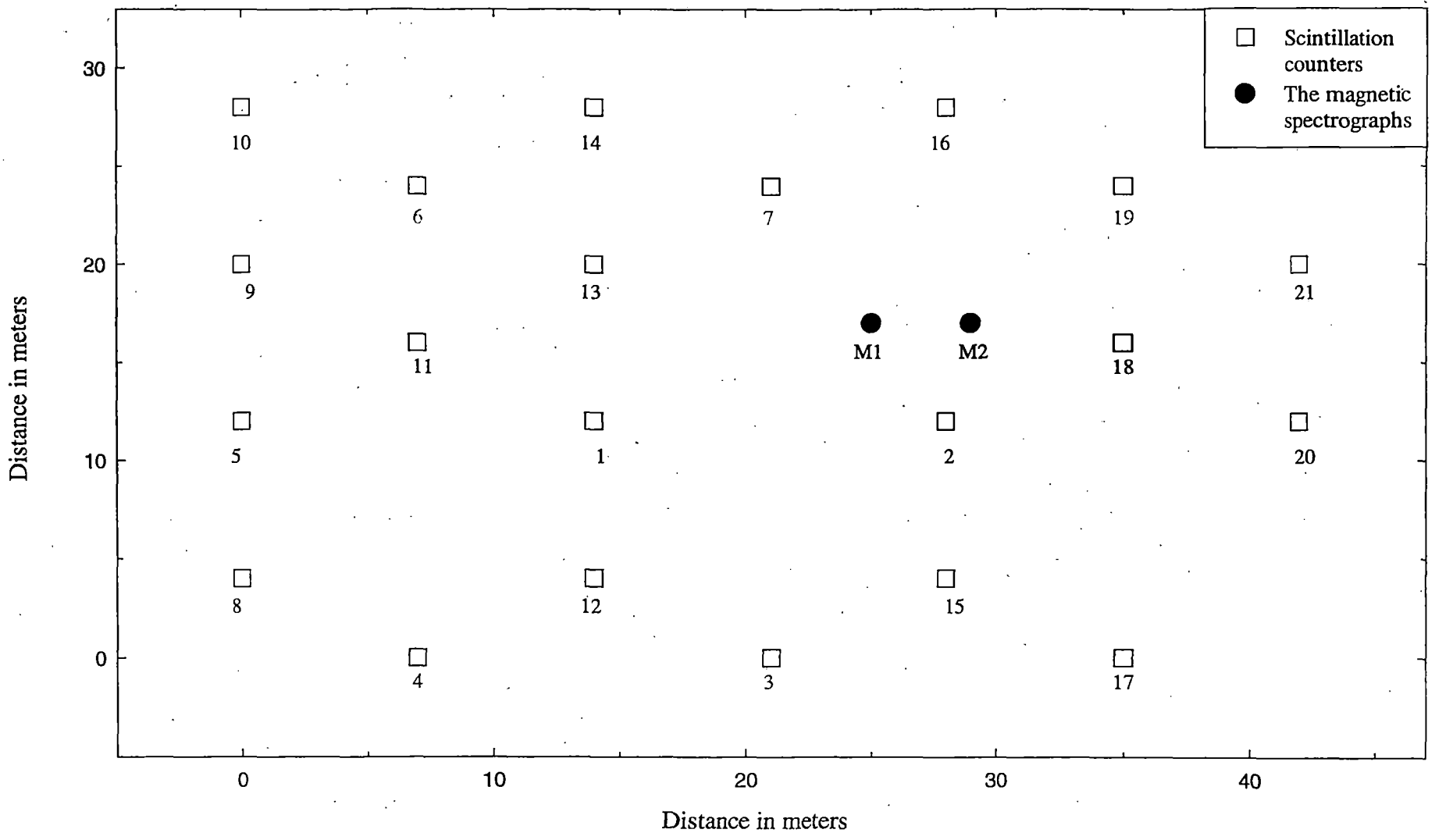

Fig. 3.1 SCHEMATIC DIAGRAM OF N.B.U. AIR SHOWER ARRAY.

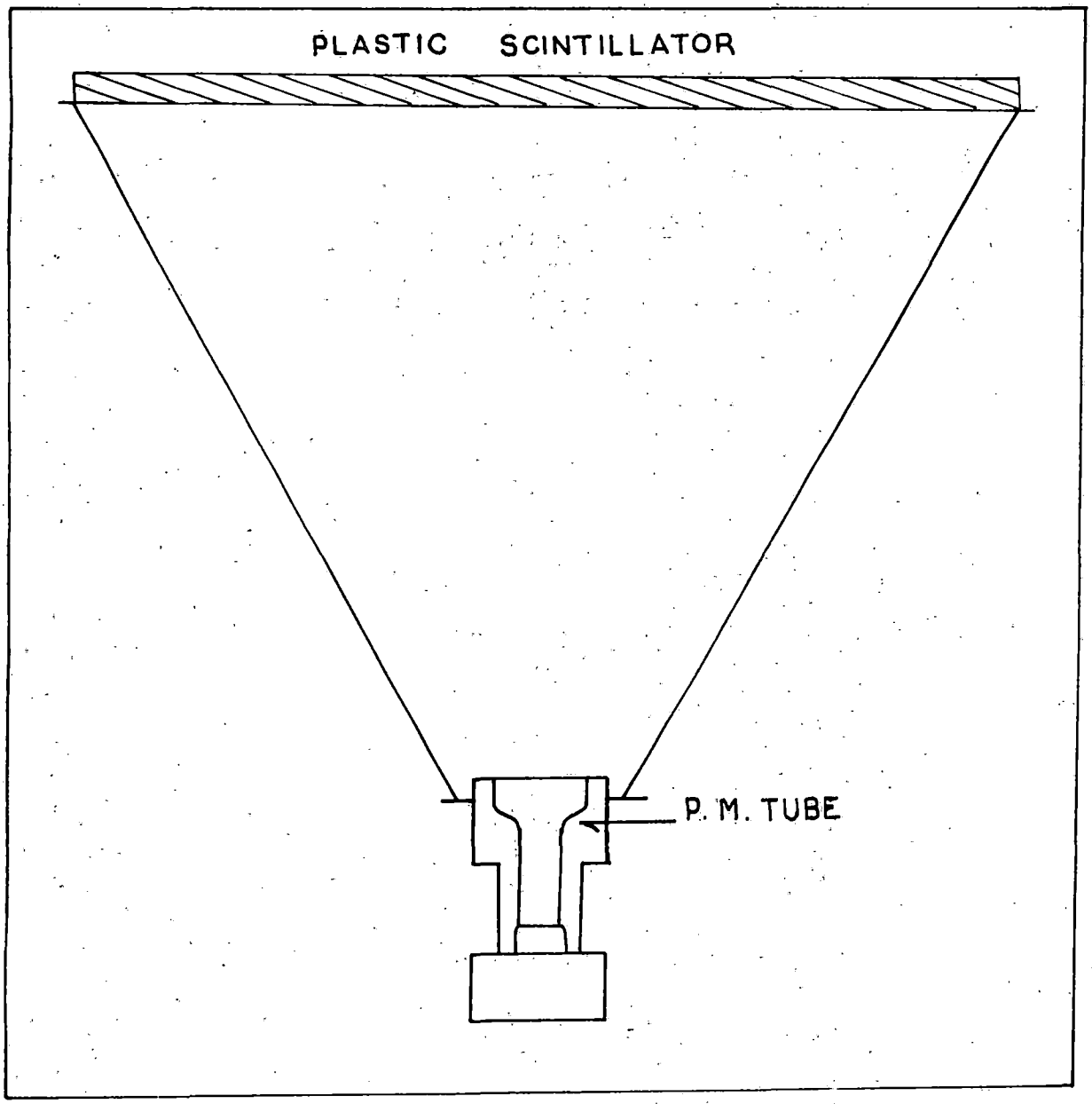

Fig. 3·2. Schematic diagram of plastic scintillation detector.

that those with smaller area were placed near the center of the array. The relative positions of counters were as shown in fig. 3.1. The other unit comprising of two magnetic spectrographs was used for the detection of muons associated with the air showers recorded by the array. These spectrographs measure the momenta of muons by measuring the deflection suffered by them while passing through the electro-magnets of the spectrographs. The design of the spectrographs is such that it restricts the zenith angle of acceptance of the incident shower to near vertical.

3.1.1 THE SCINTILLATION COUNTERS

The scintillation counters used in the array for measuring the densities of electrons are made with the plastic scintillators fabricated at Bhaba Atomic Research Centre, Bombay, India. The plastic scintillators, used in each of the detector, have a thickness of 5 cm. and are mounted firmly within a light tight aluminium holder with the shape of a pyramid. A photo-multiplier tube (brands used are DUMONT 6364, DUMONT 6292, EMI 9757, RCA 5819 and PHILIPS XP2050) is mounted suitably to view the scintillator. The schematic diagram of a scintillation detector is shown in fig. 3.2.

The pulses generated in each of the 21 detectors by the particles of the arriving showers are first amplified by a preamplifier of gain 30 and are then sent to the main laboratory where they are again amplified by main amplifier. The main amplifier preserves the original shape after amplification up to the saturation value of 10 volts. In the next stage, these pulses are fed to the 'Sample and Hold' circuit. The 'Sample and Hold' circuit, described previously in detail by Goswami et al. [4], keeps the peak value of the pulse stored for about 3 μsec by charging a condenser. After 3 μsec, if a hold pulse does not come then the condenser discharges through a transistor and is ready to accept information from the next event. The performance of each detector was studied during their calibration by measuring single particle pulse height. The variation of pulse height from the center of the detectors to their edges was observed to be within 10%.

3.1.2 THE MAGNETIC SPECTROGRAPHS

Two identical magnetic spectrographs separated by a distance of 4m have been installed in a housing at a distance of about 14m from the center of the array as shown in fig. 3.1. Each spectrograph (shown in fig. 3.3) has two constant field regions of a solid iron electro-magnet of height 1m. for the deflection of the muons,

four neon flash-tube trays (T_1,T_2,T_3 and T_4) for the location of muon trajectories and three G.M. counter trays (G_1, G_2 and G_3) for selecting vertical muons. The flashes of the tubes produced by the passing muons are recorded photographically with four cameras. Absorbers of concrete and lead plates with effective thickness of 1200gm/ cm^2 are placed at the top of each spectrograph to stop the electron component of the air showers. The whole of the magnetic spectrograph unit is shielded by G.I. mesh for screening the high voltage noise to the electronic set up, which controls the operation of array.

3.1.2(a) THE SOLID IRON MAGNETS

The electro-magnets used in each of the spectrographs consist of solid iron blocks constructed using low carbon content steel plates of 12.5mm thickness. The schematic diagram of one magnet is shown in fig. 3.4. Each plate is of size 180 X 125 cm^2 and has a rectangular hole of size 19 X 35cm^2 at the center. Eighty plates are mounted vertically one above the other on an iron framework. The two longer arms of the block are wound with 600 turns of 14 s.w.g. double cotton covered copper wire. The power requirement for each magnet when operated with 15amp current is 2.3 Kilowatts. The power supplies are fed with stabilized A.C. source and high wattage D.C. rectifier (incorporated with reversing switches for the reversal of the direction of the current). The temperature of the coil, when current is passing through them in full strength was observed to range between 34°C and 42°C for an initial room temperature of 30°C.

During the installation of the plates, secondary wires (22 s.w.g.) of single turn are wound around each group comprising of five plates at different places of the magnets in order to make provision for the measurement of magnetic field in these regions.

3.1.2(b) MEASUREMENTS OF THE MAGNETIC FIELDS

The magnetic field produced by the electro-magnets of the spectrograph was measured by a calibrated fluxmeter [3]. The circuit used for the measurement is shown in fig. 3.5. The search coils wound around each group of five plates at different places of the magnet are shown as S in the figure. The calibration of the fluxmeter was done with a 10mH fixed mutual inductance coil.

The stability of the magnetic flux was tested by studying the variation of magnetic field (B) with the excitation current (I). The ratio 'F' of fractional change in

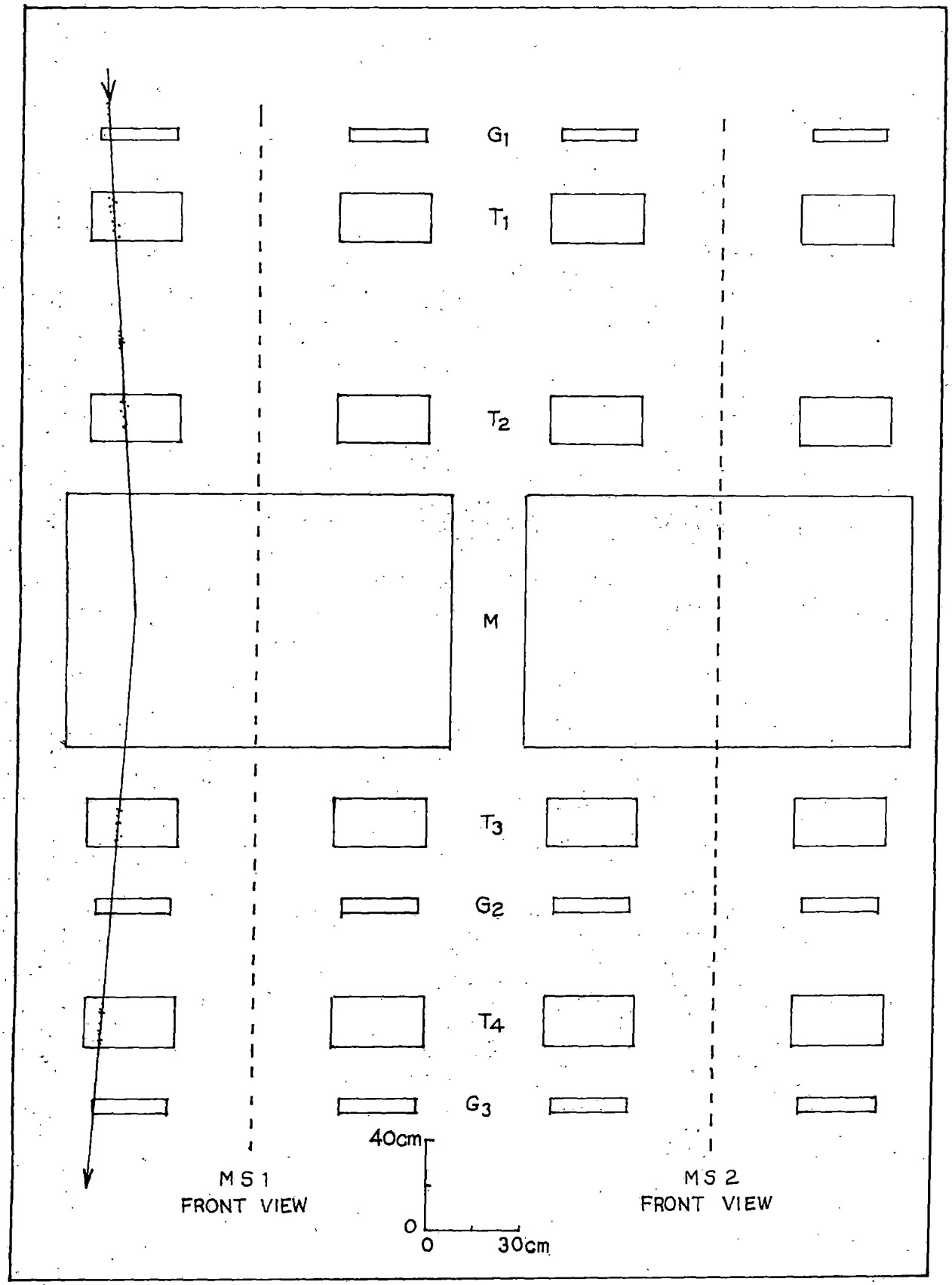

Fig.3.3. Schematic diagram of magnetic spectrograph units.

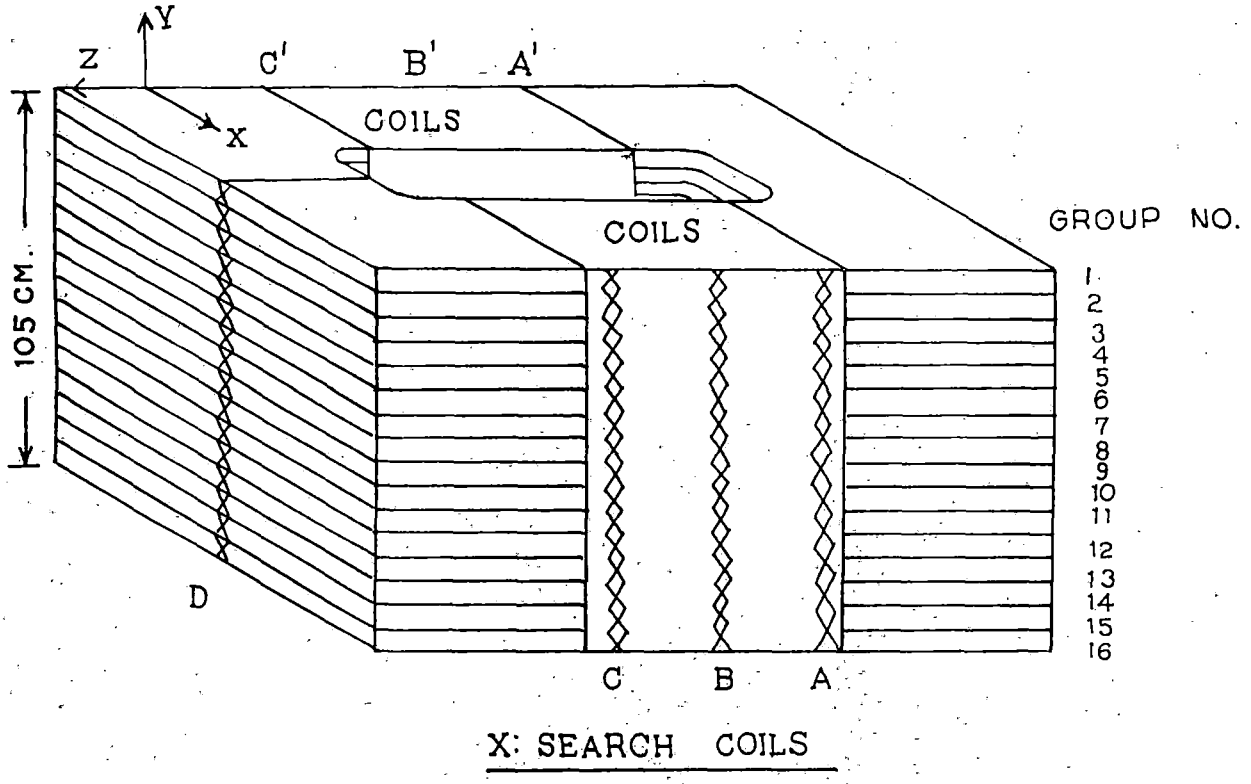

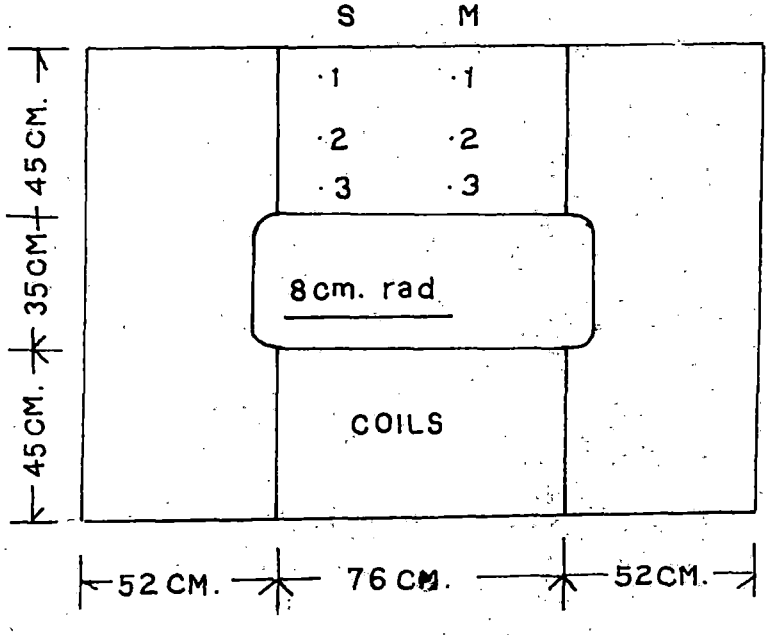

Fig 3.4 Schematic diagram of a Solid Iron Magnet.

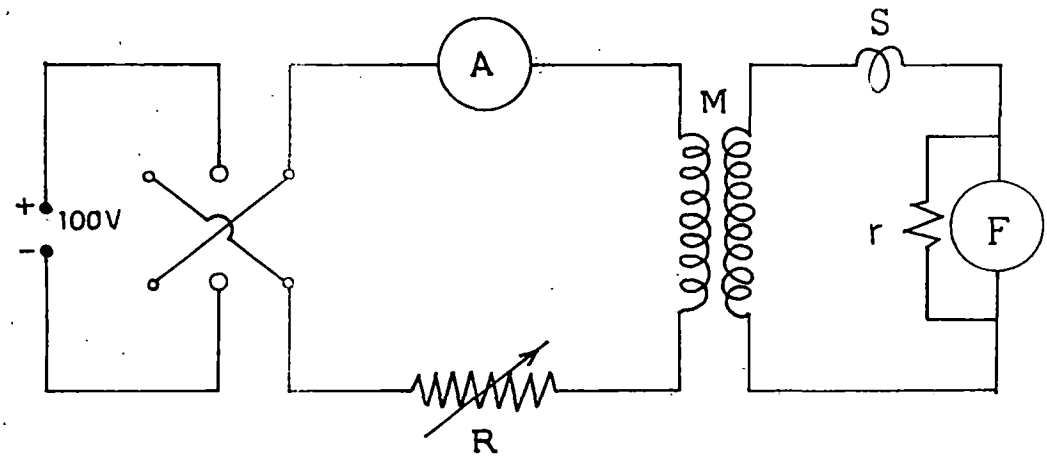

M : 10 mH

r : 1 Ohm

Fig. 3·5. Circuit diagram for calibrating the Fluxmeter(F) and for measuring magnetic field (r = Shunt resistance , S = Secondary coil of the magnet.)

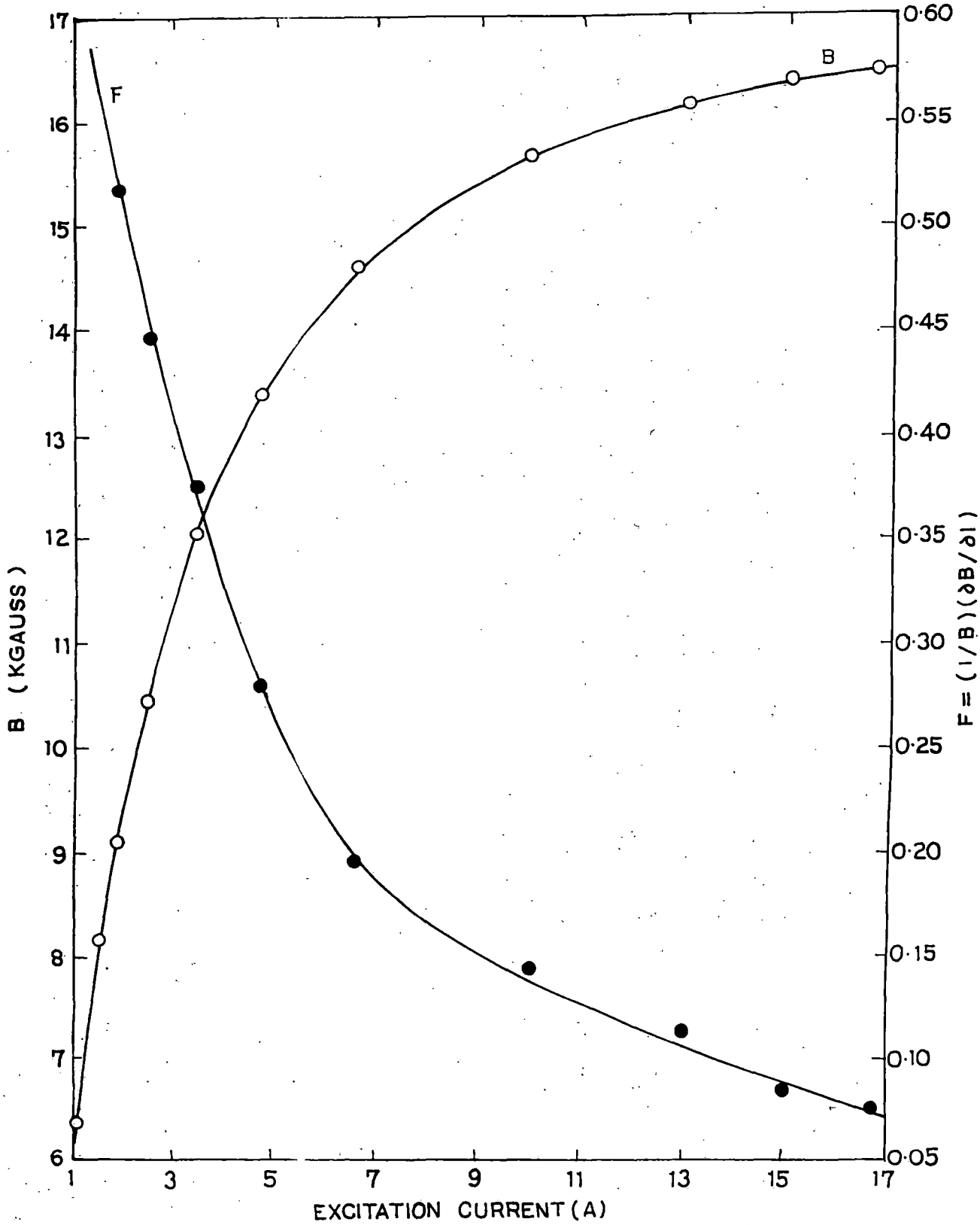

Fig.3·6. The variation of magnetic field B and $F(=\frac{I}{B}\frac{\partial B}{\partial I})$ with excitation current .

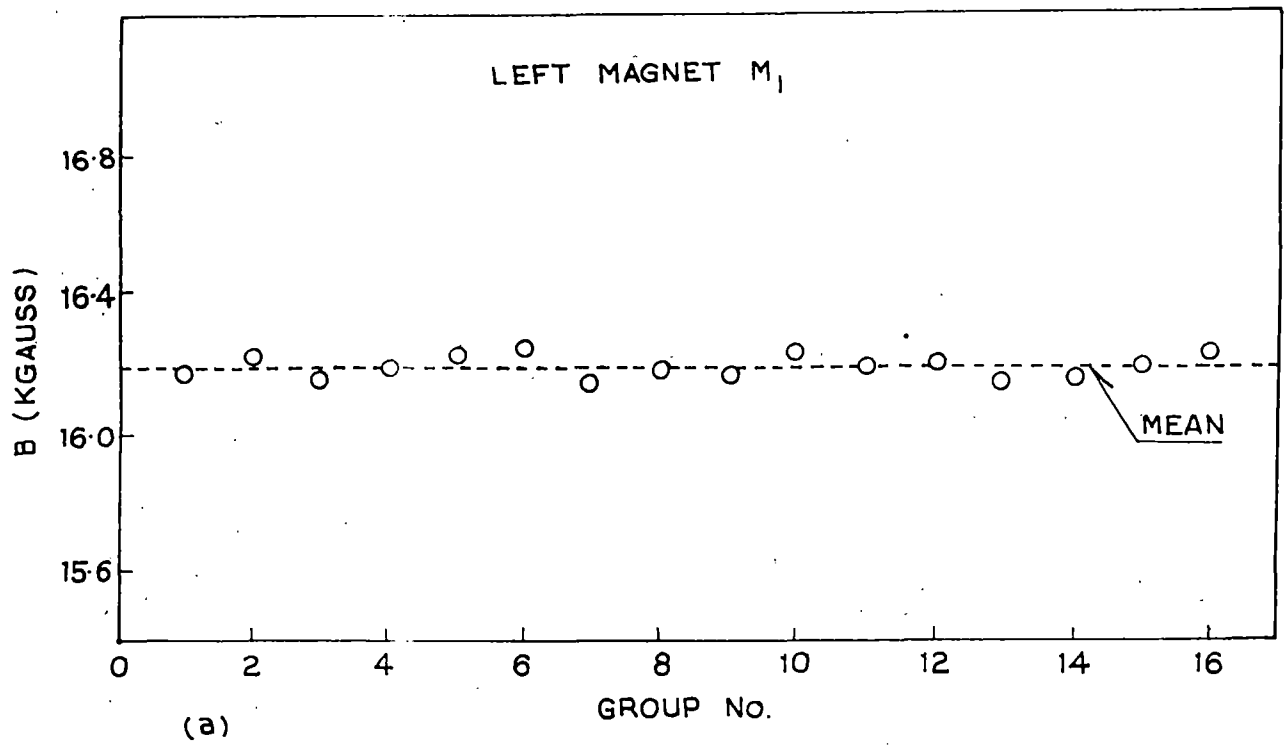

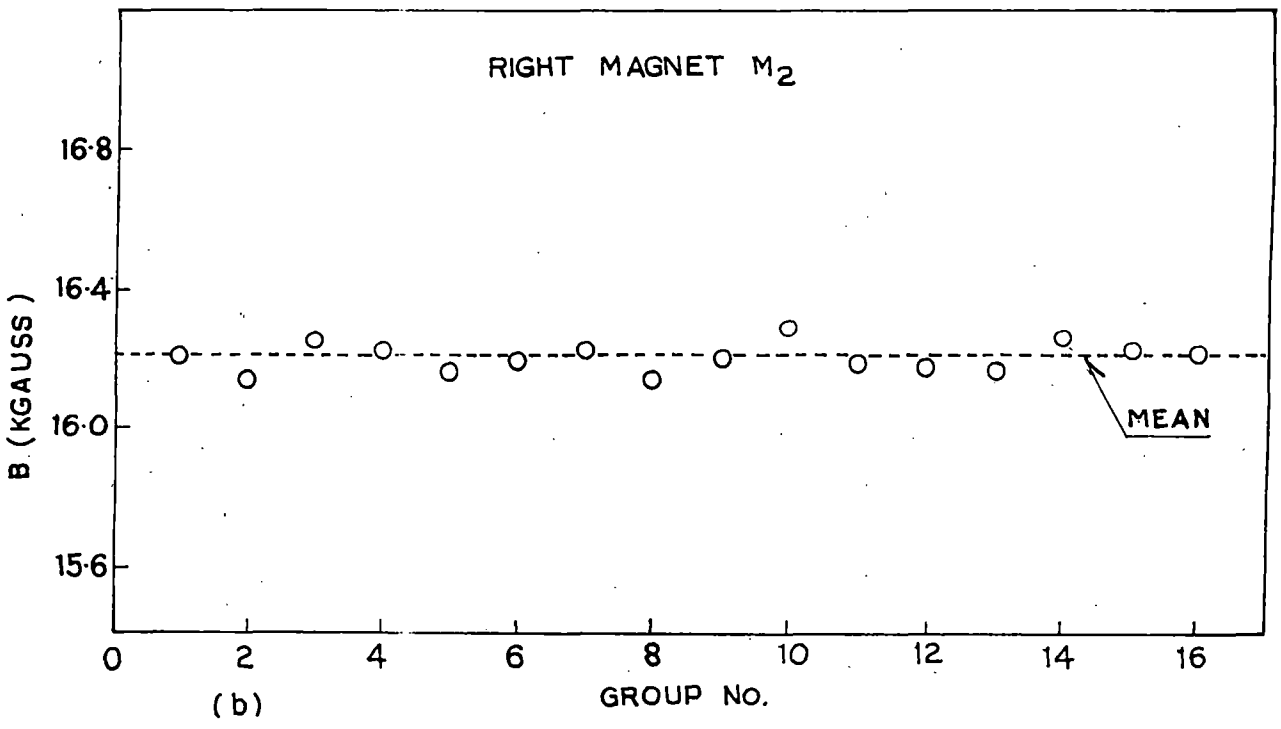

Fig 3.7 The plot of magnetic field B against group numbers of the wound arms of the magnet [mean value from six search coils A, B, C and A′, B′, C′ (Fig 3.4)]. (a) left magnet (b) right magnet.

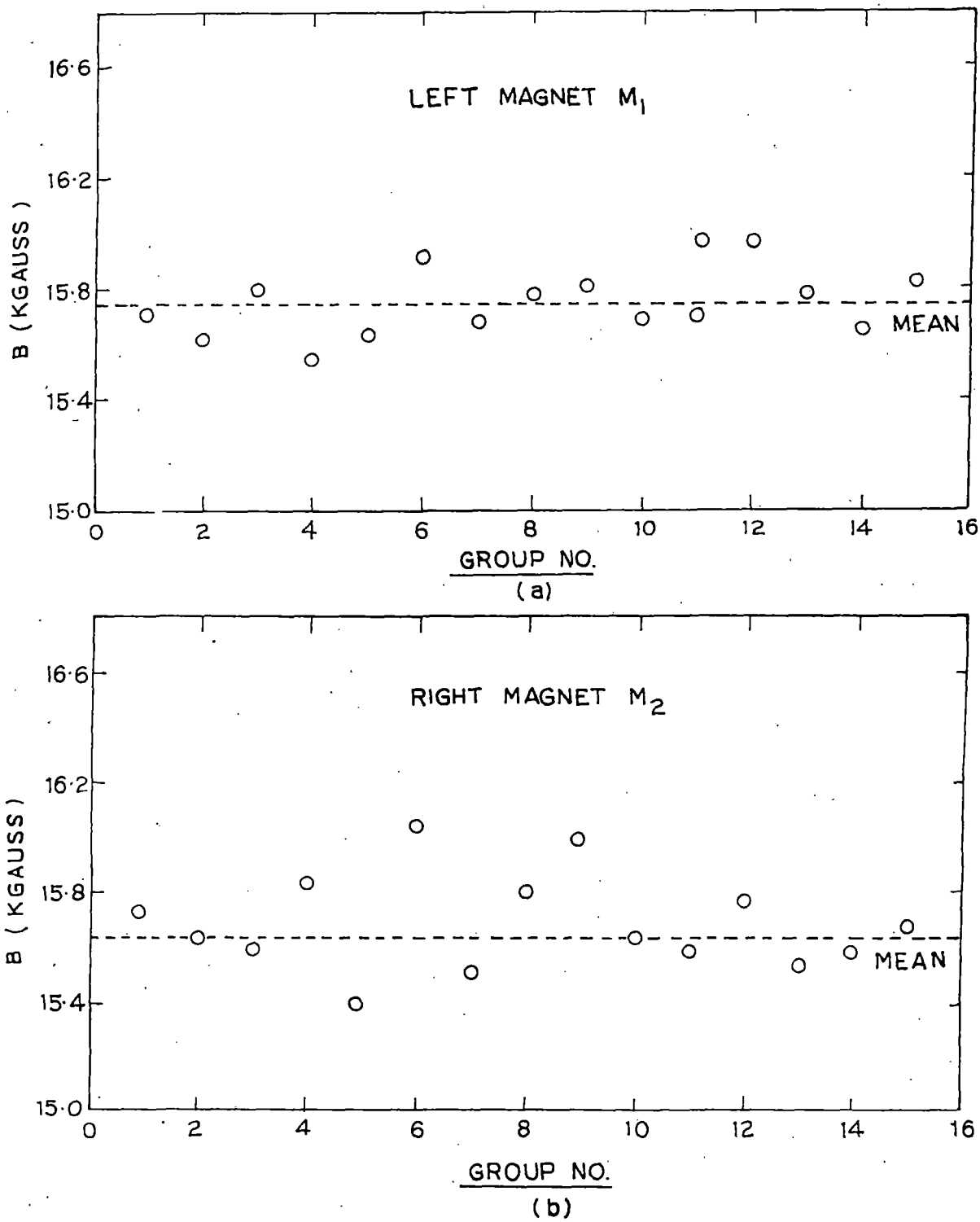

Fig. 3·8. The plot of magnetic field B against group numbers of the unwound arm of the magnets (a) Left magnet (b) Right magnet .

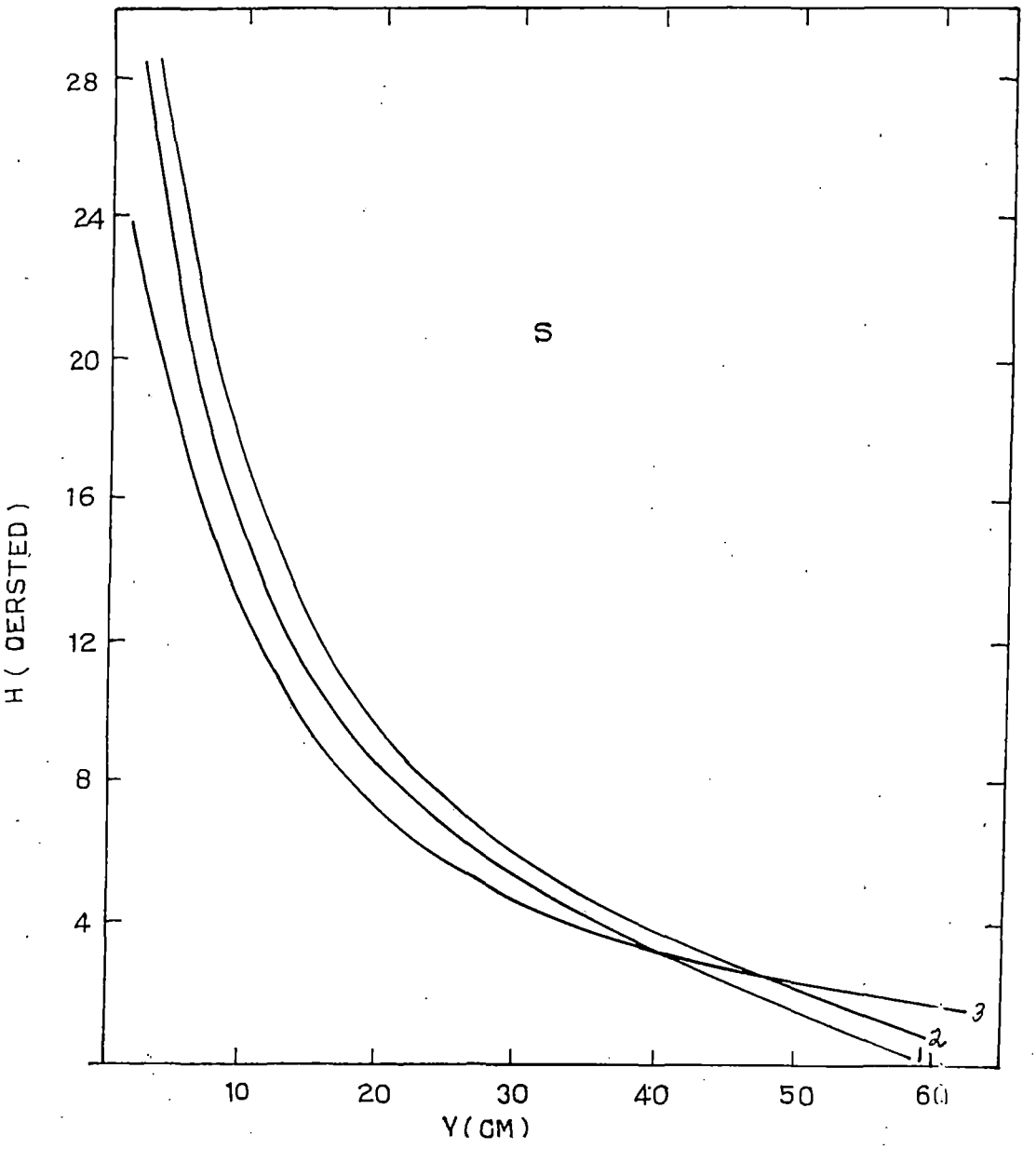

Fig. 3·9 The variation of Leakage field (H) with height above the magnet at S of Fig. 3-4 .

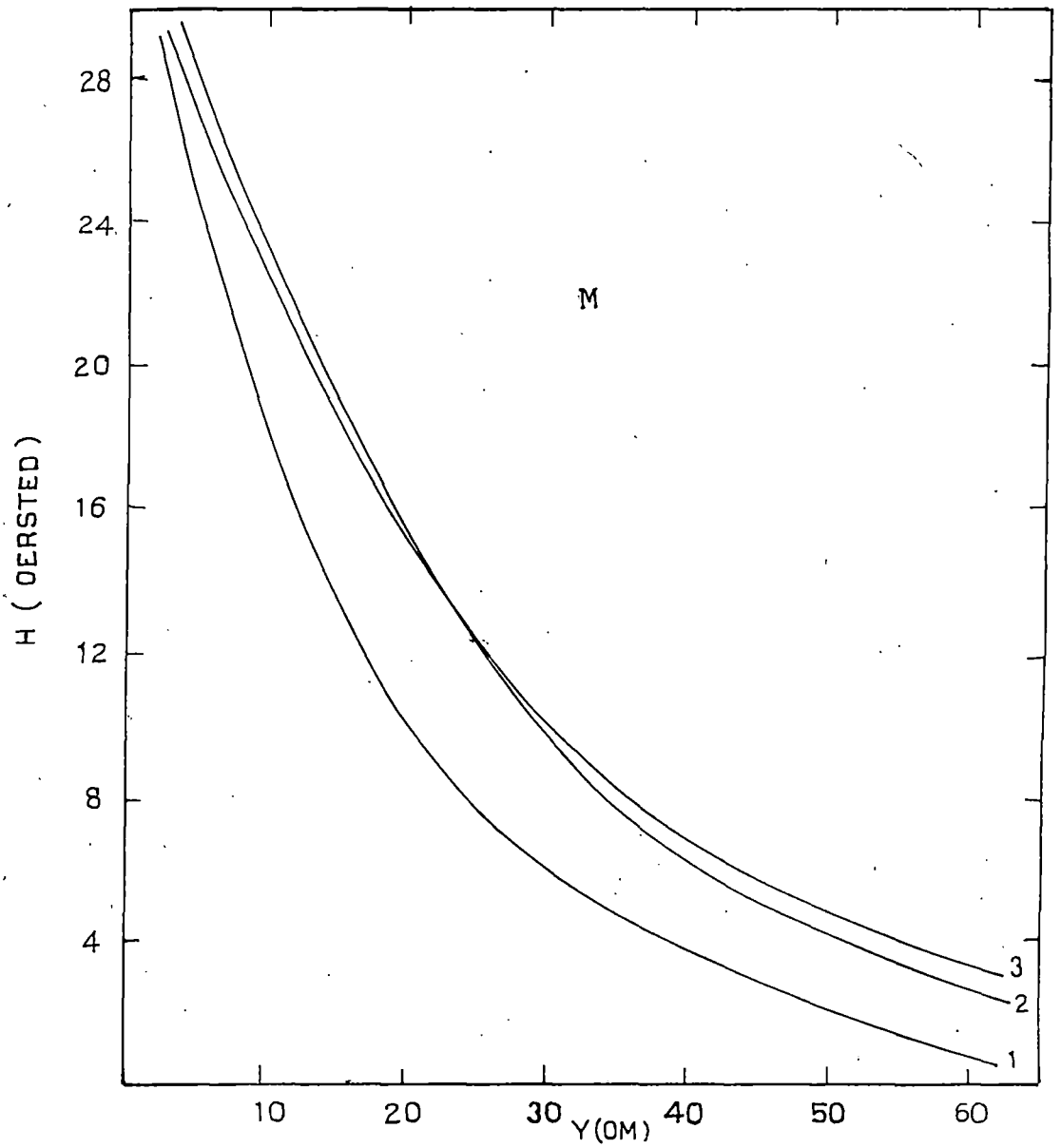

Fig. 3.10 The variation of leakage field (H) with height above the magnet at M of Fig. 3·4 .

field ∂B/B to that of current ∂I/I, which determines the stability of the magnetic flux against variation of current, is minimum when the iron is completely saturated. The observed variations of the ratio F and magnetic field (B) with excitation current are shown in fig. 3.6. The choice of the actual operating current was made in such a way that the ratio F corresponding to that particular value of current was as low as possible and the production of heat was also not high. An excitation current of 15amp was observed to be the most optimum, and with that current the corresponding value of F was seen to be about 0.1.

To study the uniformity of magnetic field throughout the iron, measurement of magnetic flux was made on each group of five plates in the wound and unwound arms. The mean results for wound arms of left and right magnets are shown in fig. 3.7 and that for unwound arms in fig. 3.8. The mean value of magnetic fields from 16 groups of wound and unwound arms were measured to be respectively 16.2 K gauss and 15.9 K Gauss. From these figures it is clear that the magnetic field inside the iron was sufficiently uniform and it could be pointed out that the apparent non uniformity (less than 2%) was due to the slight variations in the dimensions of the steel plates.

The magnetic field extending in the air above the surface of the magnet, the so-called leakage field, was measured by rotating a search coil with the operating current of 15amp. The variation of the leakage field (H in Oersted) with height above the magnet was observed as shown in fig. 3.9 & 3.10 at three different positions indicated as 1,2, & 3 in the fig. 3.4. The line integral of the leakage field was found to be 0.04% of the field produced within the iron. And hence, the effect of leakage field on the trajectories of muons was considered to be negligible.

3.1.2(c) THE NEON FLASH-TUBES

The trajectories of the muons passing through the magnetic spectrographs are located with the help of neon flash tubes. Multi-layered trays of flash tubes are arranged both above and below the electro-magnets of the spectrograph and the flashes produced in the tubes by the passage of each muon through them are recorded photographically. Before describing the arrangement of flash tubes in the spectrographs, a few things about their general characteristics and their operation are discussed here.

A neon flash tube is an ordinary glass tube filled with neon gas whose one end has a flat window for observing the glow or the flash produced by the discharge in the

tube. The sides of the tubes are painted black to shield the light coming from outside and the adjacent tubes. These types of tubes were first used as charged particle detectors by Conversi and Gozzini [5] for the location of high energy cosmic ray particles and were further developed by Barsanti et al. [6] and Gardner et al. [7].

The passage of a charged particle through the tube ionizes the gas inside it causing the emission of secondary electrons. If a very high electric field is applied on to the tubes within a very short interval of time after the passage of the particle then the field further accelerates the secondary electrons. Thus the electrons gain sufficient energy to produce more secondary electrons thereby an electron avalanche is produced. As a result almost the whole of the atoms are excited. The excited atoms return to their ground states resulting in a luminous discharge in the tubes which is recorded photographically.

The performance of a flash tube is described in terms of its efficiency, which is defined as the probability of initiating luminous discharge by the passage of an ionising particle. For practical purposes the efficiency is defined in two ways - the layer efficiency and the internal efficiency. The layer efficiency is the ratio of number of single flashes observed in a layer and the number of particles traversing through that layer. And, the internal efficiency is defined as the product of layer efficiency with the ratio of the separation of tube centers and the internal diameter of the tubes. These efficiencies of the tubes basically depend upon two factors - (i) the nature and the purity of the gas used in the tubes and (ii) the parameters characterising the high voltage pulse applied to the tubes, such as the pulse height, the rise time, the delay time and the pulse width. However, Gardener et al. [7] has pointed out that there is no significant difference in efficiencies of the tubes filled with spectroscopic neon and those filled with commercial neon gas. It was also observed that the efficiency does not depend on the length of the tube but it falls very rapidly if the diameter is decreased. The efficiency also increases with the increase of pressure.

The dependence of efficiencies of flash tubes on the high voltage pulse characteristics was studied in detail by Coxell and Wolfendale [8-9]. It was observed in their study that the probability of flashing increases with the height of the high voltage pulse but decreases with increase of delay (T_D) and rise time (T_R), of the pulse.

Some 'spurious' flashes, which are not associated with any incident particle, are also observed while working with flash tubes. These 'spurious' flashes, as pointed

out by Coxell and Wolfendale [8], are mainly due to the radioactive contamination of the glass and surroundings. The occurrence of spurious flashes increases with the increase of the electric field as smaller number of electrons are also sufficient to initiate the discharge when the applied electric field is high.

So, with all these observations of different authors, it can be pointed out here that for the maximum efficiency of the flash tubes the rise time, the delay time and the width of the high voltage pulse should be as small as possible. And at the same time the high voltage pulse should be such that it causes minimum of spurious flashes. During the performance of the present experiment the rise time, the delay time and the width of the high voltage pulse applied to the neon flash-tubes were ~0.5μsec, ~10μsec and ~6μsec respectively.

The two magnetic spectrographs have four limbs of magnets, two in each one of them. And, each limb has four trays of neon flash tubes, indicated as T_1,T_2,T_3 and T_4 in the fig.3.3, for the location of particle trajectories. Each tray of flash tubes consists of 120 neon flash-tubes. These tubes are arranged in eight layers containing 15 tubes in each of them. The tubes in each layer are staggered in such a way that a single particle passing through a tray must traverse at least four tubes. The staggering arrangement of the flash tubes in a tray is shown in fig. 3.11. The tubes in each tray are supported on slots milled accurately in 'duraluminum' bars by means of a milling machine at 'Central Mechanical Research Institute', Durgapur, India. Thin aluminum electrodes (1 / 32") are placed in between the layers of tubes. The horizontal separation of the tube center is 1.999 ±0.002 cm which is referred to as one tube separation (t.s.). The vertical separation between the tube center in a pair of adjacent layers is 2.8 cm. The general characteristics of the tubes used in the magnetic spectrographs of NBU array are summarised in Table- 3.1.

3.2 Electronic Control System of the Array

The electronic system that controls the operation of whole air shower array for detection and recording of the air shower events incident over it, was designed and fabricated by the earlier investigators of the array and is described in detail by them in [3,4 & 10]. The system basically consists of two different units working in conjunction with each other. The first unit selects the shower event that satisfy the required coincidence criteria and records the electron density information collected by the array of scintillation counters. The other unit controls the magnetic spectrographs,

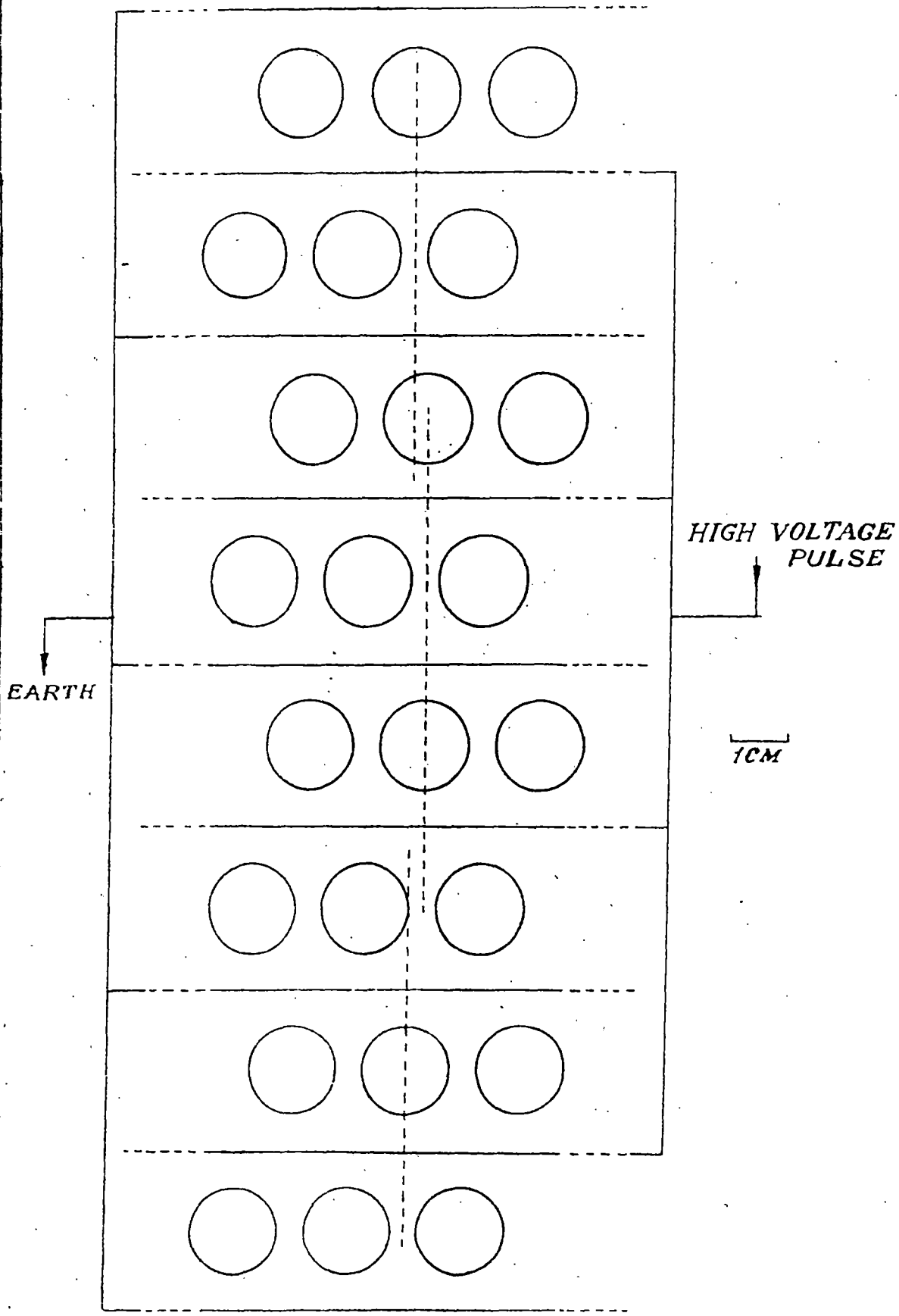

Fig. 3.11 THE STAGGERING ARRANGEMENT OF THE FLASH-TUBES IN A TRAY OF MAGNETIC SPECTROGRAPH.

which detect the muon component of the shower and records data related about the momentum of the muons.

Table-3.1: Characteristics of the neon flash-tubes used in the magnetic spectrographs of NBU air shower array

Internal diameter	1.55 cm
Glass	Soda
External diameter	1.8 cm
Horizontal separation of the tube centers	1.999 ± 0.002 cm
Vertical separation of the layers	2.8 cm
Length of the tubes	100 cm and 200 cm
Gas pressure	60 cm of Hg
Average internal efficiency	99.2%
Average layer efficiency	76.9 %

3.2.1 Shower Selection and Electron Density Measuring System

The system that selects the air shower events and records the information about the densities of electrons detected by the scintillation counters is shown in fig.3.12. Pulses from each scintillator are amplified to a desired amount and then discriminated with adjustable biases by which the level of response for each detector can be set to any desired counting rate. These counting rates correspond to certain minimum densities of particles in the detector. The criteria for shower selection is based on three-fold coincidence between the pulses coming from any two adjacent detectors among the six selected detectors (detectors numbered as 2 to 7 in fig. 3.1) and the central detector (detector numbered as 1 in fig. 3.1). The threshold density of electrons for each detector is 4 particles per m^2. This coincidence generates a master pulse that operates the electronic system which records the electron densities measured by individual detectors on a paper tape.

The amplified analogue output from all 21 detectors of the array are fed to the 'Sample and Hold' circuits by charging capacitors for 3μsec. which discharges through a transistor if no master pulse triggers on the Master Control Unit (MCU). On the other hand, if the MCU is triggered by the master pulse then it gives a hold command to the sample and hold unit, and at the same time switches off the input lines, gates off the coincidence circuit from the MCU and sends a start pulse to the programmed ADC (Analogue-to-Digital Converter) and the memory program unit. All the input lines are connected to FET switches for disconnecting input lines from Sample and

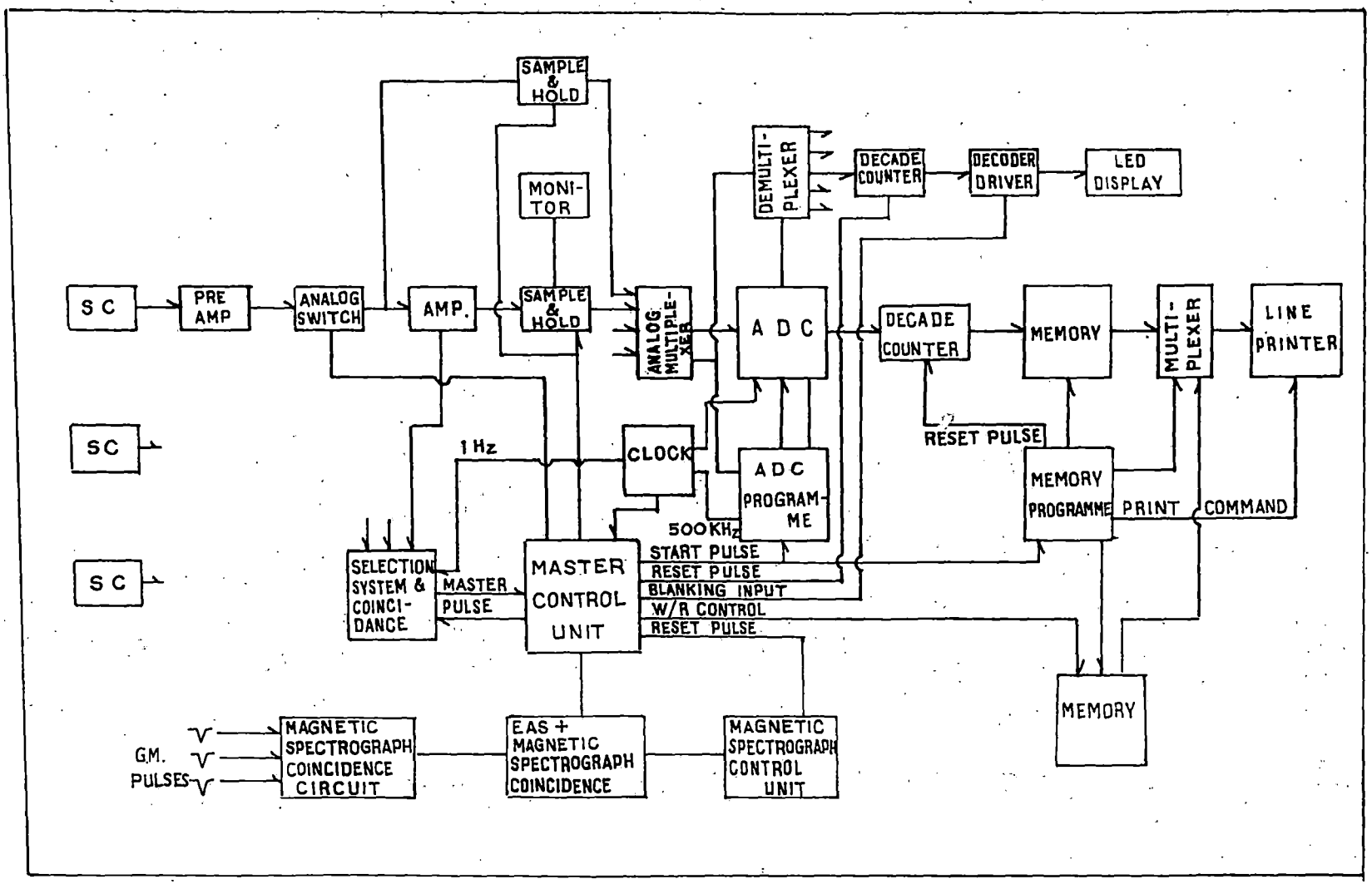

Fig. 3·12. Block diagram of electronics of AIR SHOWER ARRAY

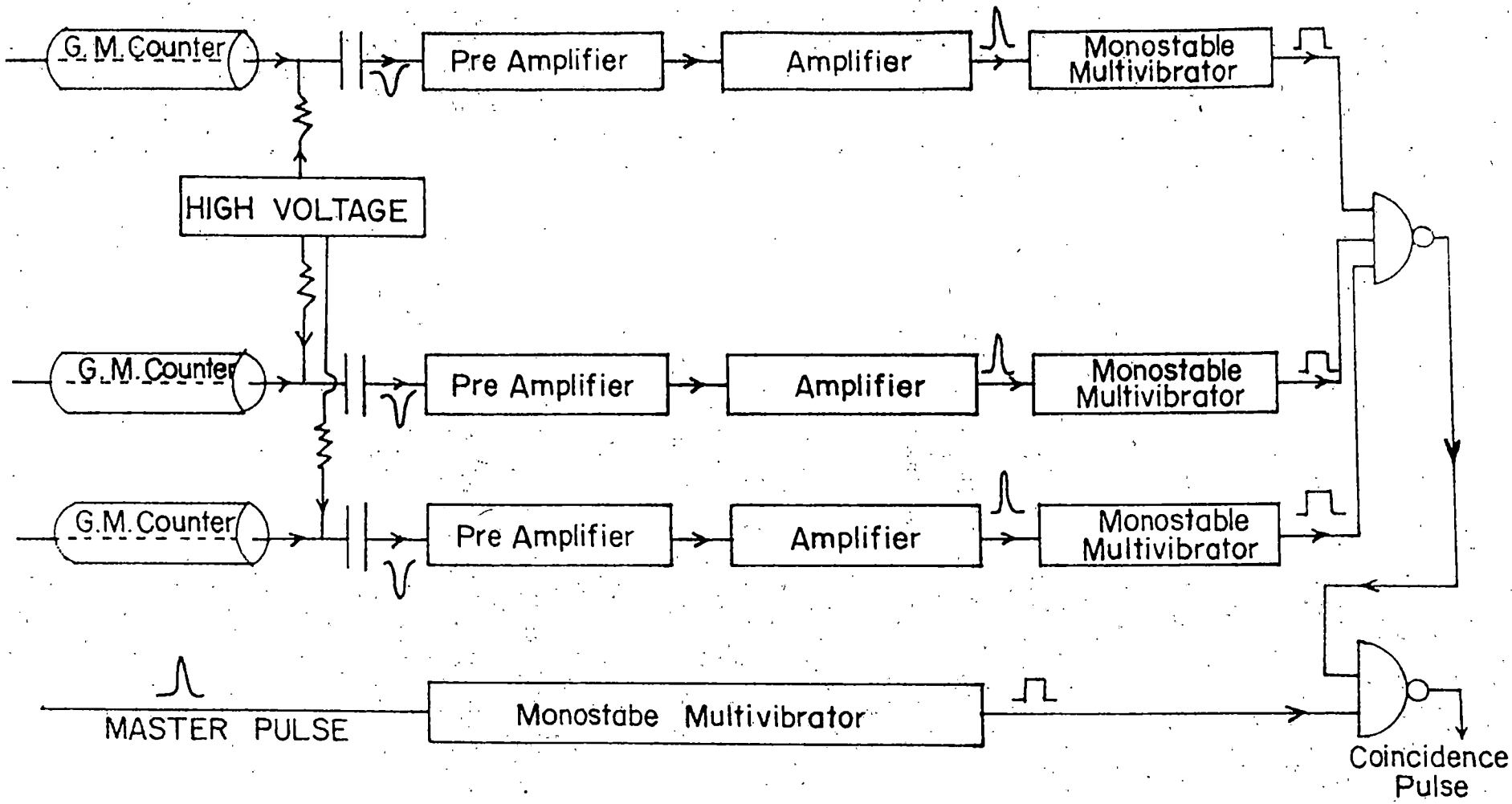

Fig. 3.13 BLOCK DIAGRAM OF COINCIDENCE CIRCUIT AND TRIGGERING SYSTEM OF THE MAGNETIC SPECTROGRAPHS.

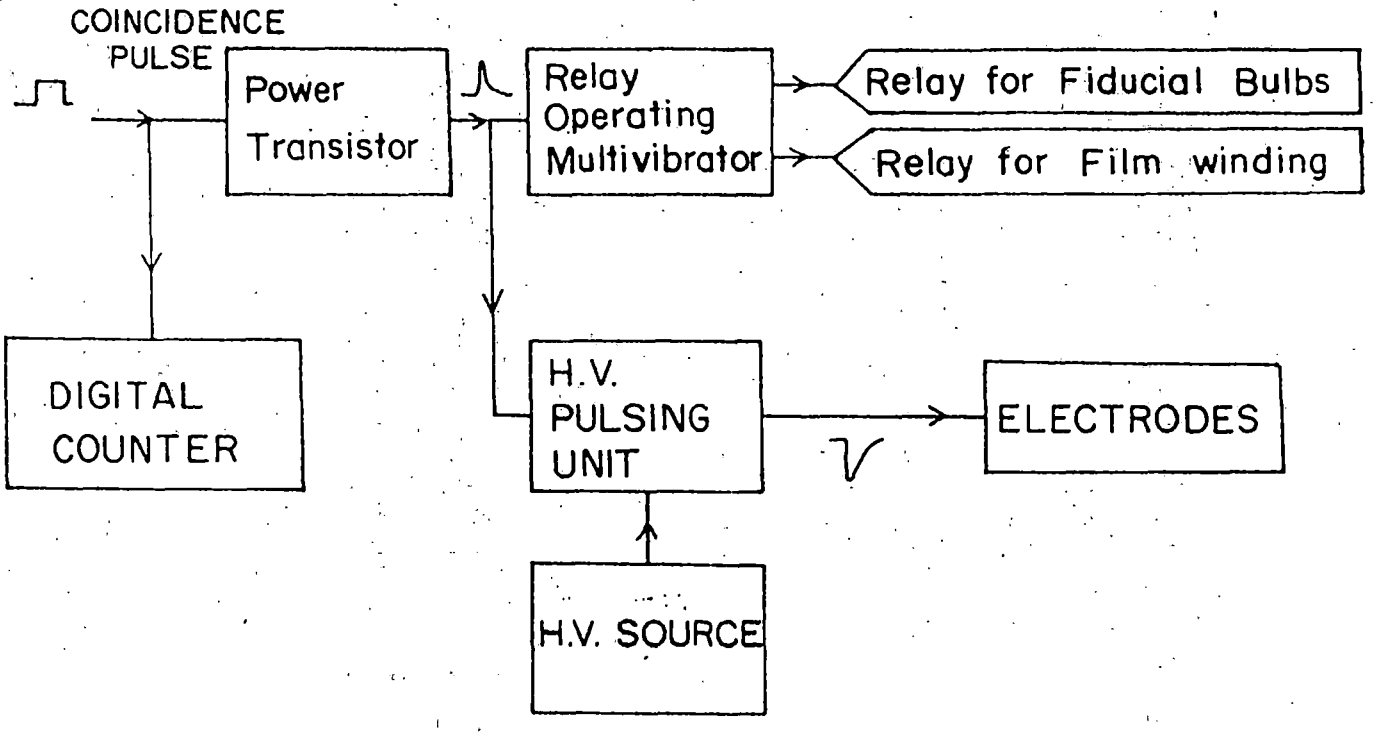

Fig. 3.14 BLOCK DIAGRAM OF MAGNETIC SPECTROGRAPH CONTROL UNIT

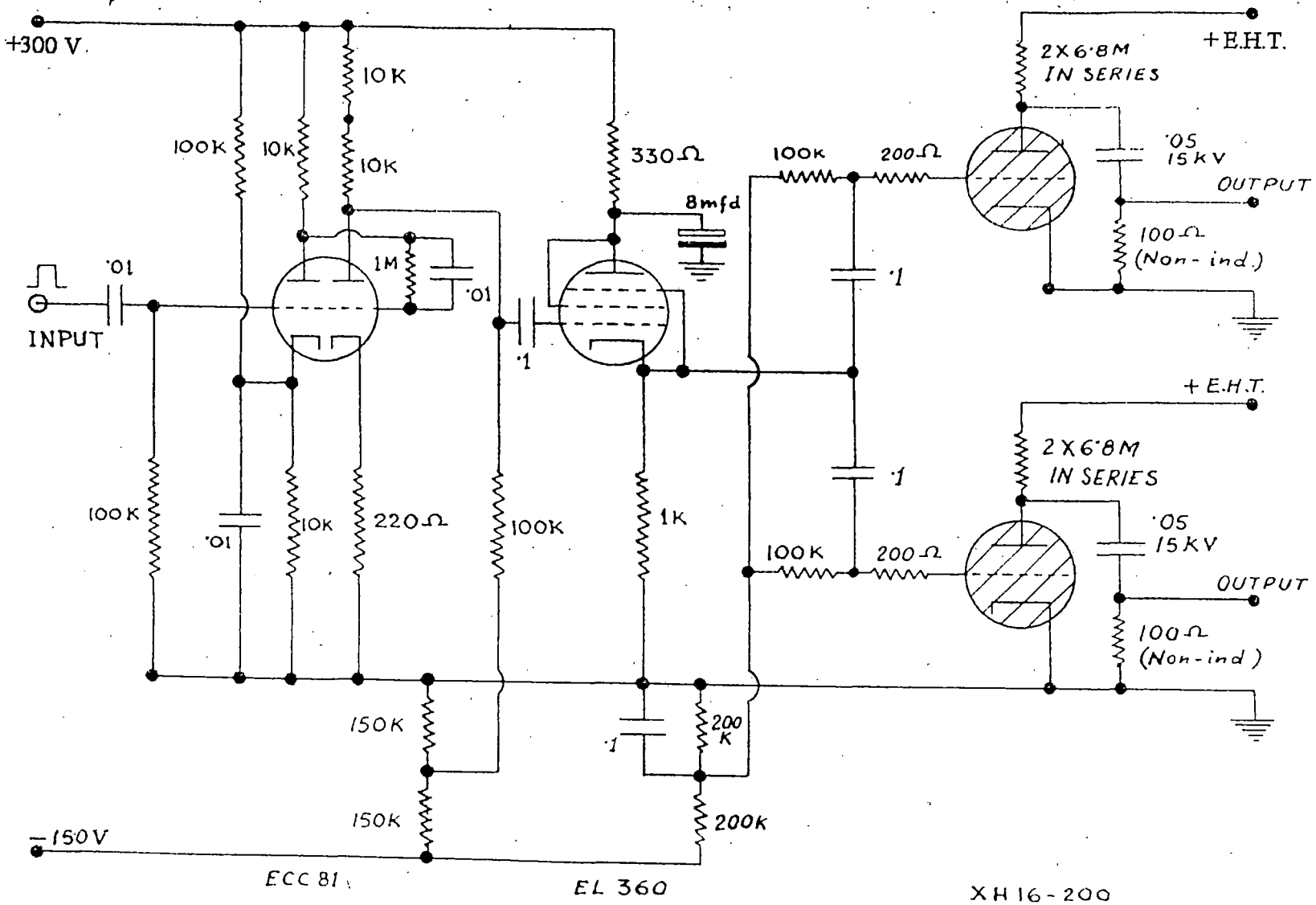

Fig. 3.15 THE CIRCUIT DIAGRAM OF THE HIGH VOLTAGE PULSING UNIT.

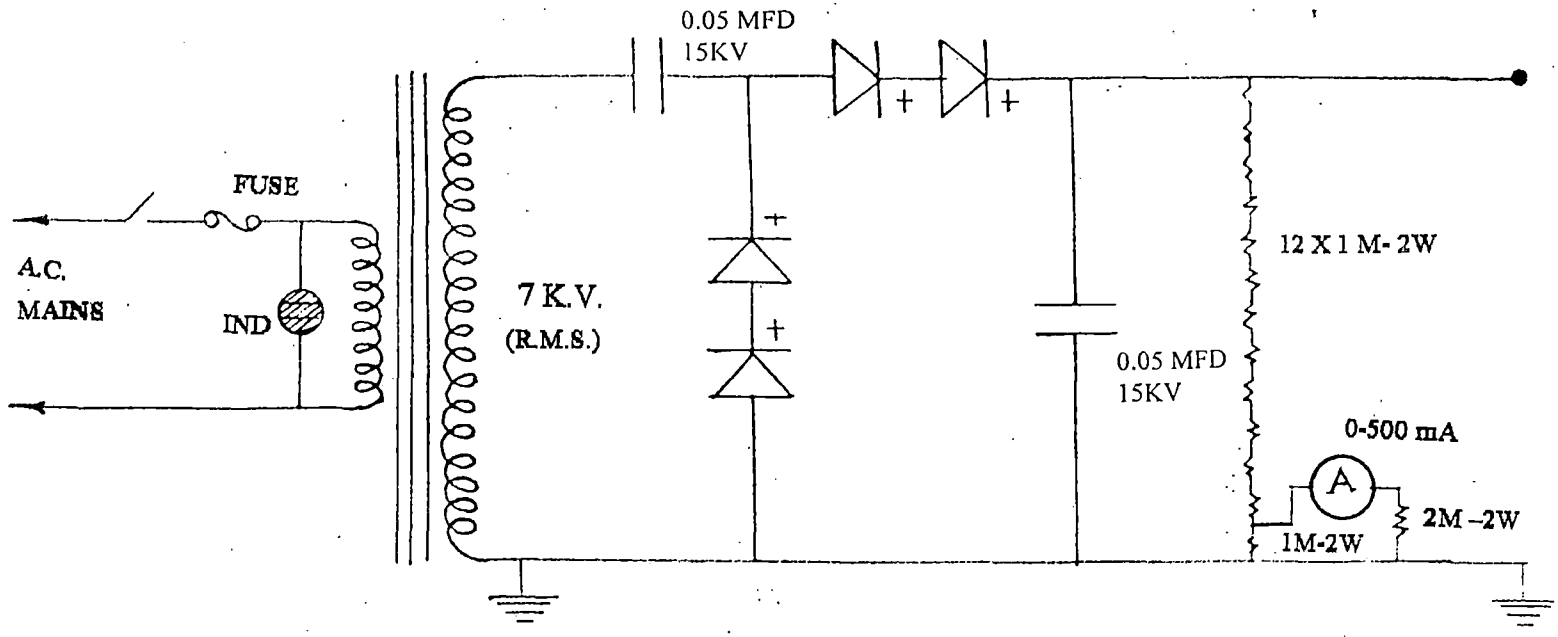

TRANSFORMER: INPUT - 220V AT 50 C/S
OUTPUT- 7 KV (R.M.S.) AT 5 mA.
RECTIFIERS : 4 X S.T.C. K8/140
CAPACITORS : 0.05 MFD/ 15 KV

Fig. 3.16 THE CIRCUIT DIAGRAM OF THE HIGH VOLTAGE D.C. POWER SUPPLY.

Hold during the data conversion time. Hold command cuts off the coincidence circuit for 33-sec. (paralyzing time) which is controlled by MCU. Once ADC program unit is triggered, it connects all the pulses at the output of the sample and hold circuits by the analogue-multiplexer one after another to the ADC. The total time necessary to scan all the channels is about 8 msec. After scanning the first channel the ADC gives a write pulse to the memory for writing the digital information in the memory. As soon as the counting in the first channel is over, the ADC program initiates the multiplexer to connect the second channel and write the digital information to the memory in the similar way. The NBU air shower data-handling system has a provision to detect density from 32 channels but at the time when the present experiment was performed 21 detectors were in use. So, after the completion of scanning and writing for 32 channels, a read pulse is generated from the memory program unit which in turn operates on the memory unit for recording the digital information on a paper tape by a line printer. All these processes are completed within 12 sec after coincidence trigger. After 33 sec the analogue switch is opened and it switches on the input lines for the next event. Paralyzing time is made high for the operation of magnetic spectrograph unit.

3.2.2 The Magnetic Spectrograph Controlling System

The block diagram of the electronic circuits connected with magnetic spectrographs is shown in fig. 3.13. The G.M. pulses from the trays (G_1 G_2 and G_3) (Fig. 3.3) are first amplified by operational amplifiers and then converted into logic pulse by TTL gates. A flip-flop circuit shapes the input pulse. The G.M. pulses are first made coincident by three input NAND gate and the output of it is connected with the master pulse from the air shower triggering system by two input NAND gate for coincidence (fig.3.13). The output of the NAND gate i.e., the magnetic spectrograph and EAS coincidence pulse is then fed to the base of a power transistor (fig.3.14) for triggering the magnetic spectrograph units. The output pulse from the power transistor fires a thyratron (5c22 / XH -16-200) which in turn discharges a condenser (0.05 μf) charged to about 14 KV through a 100 ohm non-inductive resistance. The resulting high voltage pulse is then applied to the electrode plates between the flash-tube layers. Four such high voltage pulsing units supply pulses to 16 flash tube trays. The diagram of the high voltage pulsing unit is shown in fig. 3.15. The fig. 3.16 shows the high voltage D.C. power supply which supplies voltage of 14 KV to the pulsing unit. The

rise time and the delay time between the passage of the particle through the spectrograph and the application of the pulse to the flash-tube trays are 0.5 μsec and 10μsec respectively.

The same coincidence pulse from the power transistor triggers five mono-stable multi-vibrators, which in turn operate five relays. Four of these are used in winding the films in the four cameras after recording the muon event and the fifth relay is used to operate the neon fiducial bulbs which act as reference marks on the side of the trays.

3.3 CALIBRATION OF THE SCINTILLATION COUNTERS

As explained earlier in article 3.2.1, the amplified analogue output from the scintillation counters of the array are measured by the ADC through sample & hold and analogue multiplexer. And, the digital output is recorded in a paper tape by a line printer. For the correct operation of the circuit the digital output for all the channels are to be checked with reference to any one of the 21 channels. For this purpose a pulser was connected to one chosen channel and it was short-circuited with all other channels one after another. The process was repeated for all the channels. This way the digital output for all the channels were measured and compared.

For calibration of the detectors, three-fold coincidence of G.M. telescope was used to trigger for single particle passing through the scintillator. The electron density Δ is related to the digital output (D) by the relation,

$$\Delta = \frac{D}{S.M}$$

where S is the area of the detector and M is the pulse height corresponding to single particle.

The single particle pulse height was obtained from the calibration curve and was seen to have a value between 43 and 47 for all the detectors [3]. The calibration for all the detectors was checked regularly one after another taking one at a time.

Furthermore, the variation of efficiency of the detectors from their centers to the edges, observed by using the G.M. telescope at different positions, was noted to be within ± 10% as shown in fig.3.17.

3.4 ALIGNMENT OF THE MAGNETIC SPECTROGRAPHS

The magnetic spectrographs consist of 16 neon flash-tube trays, 4 in each limb of the two magnets. The alignment of each set of four trays (2 above and 2 below the

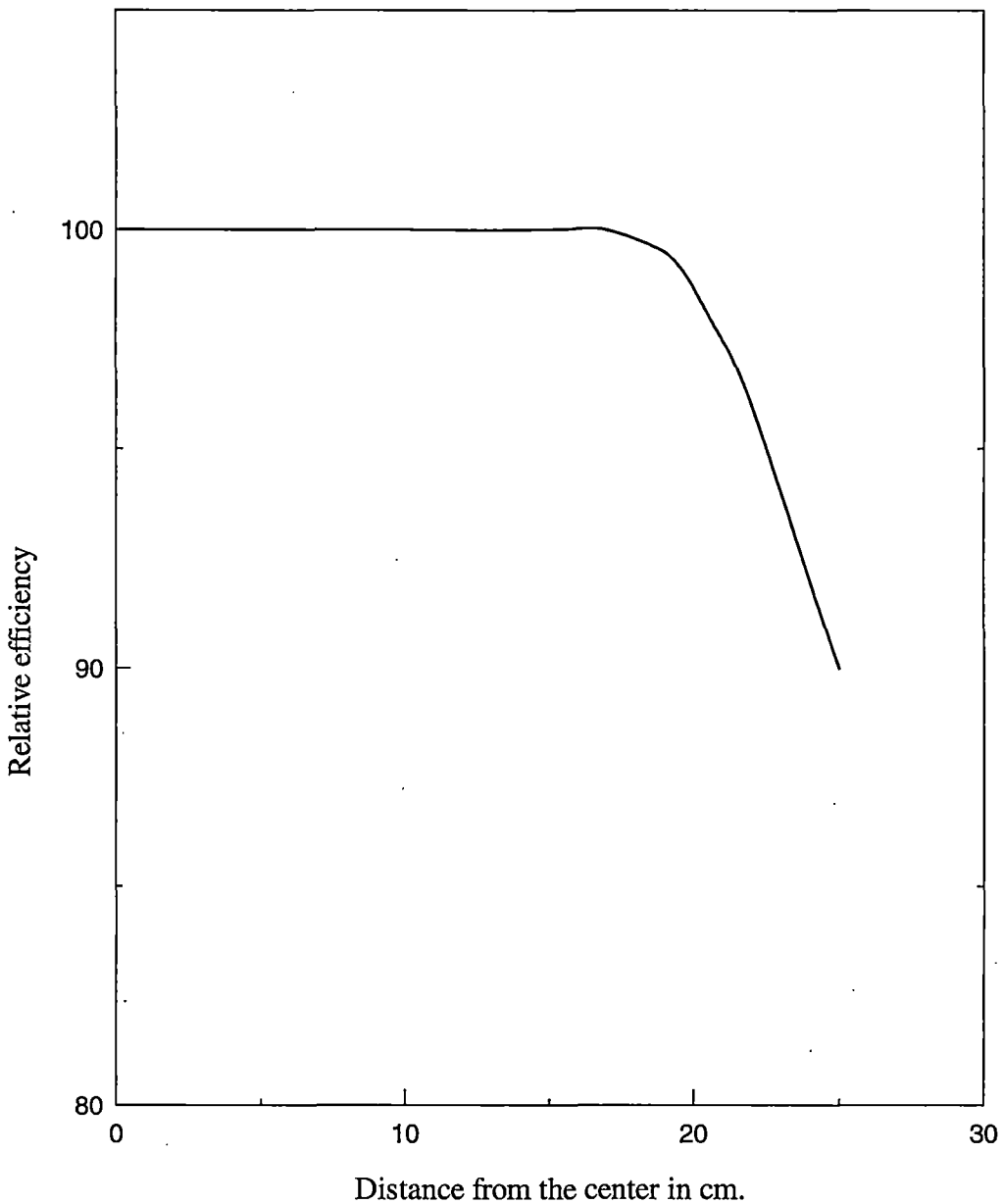

Fig. 3.17 THE RELATIVE EFFICIENCY CURVE OF THE SCINTILLATION COUNTERS AS A FUNCTION OF THE DISTANCE FROM THE CENTRE.

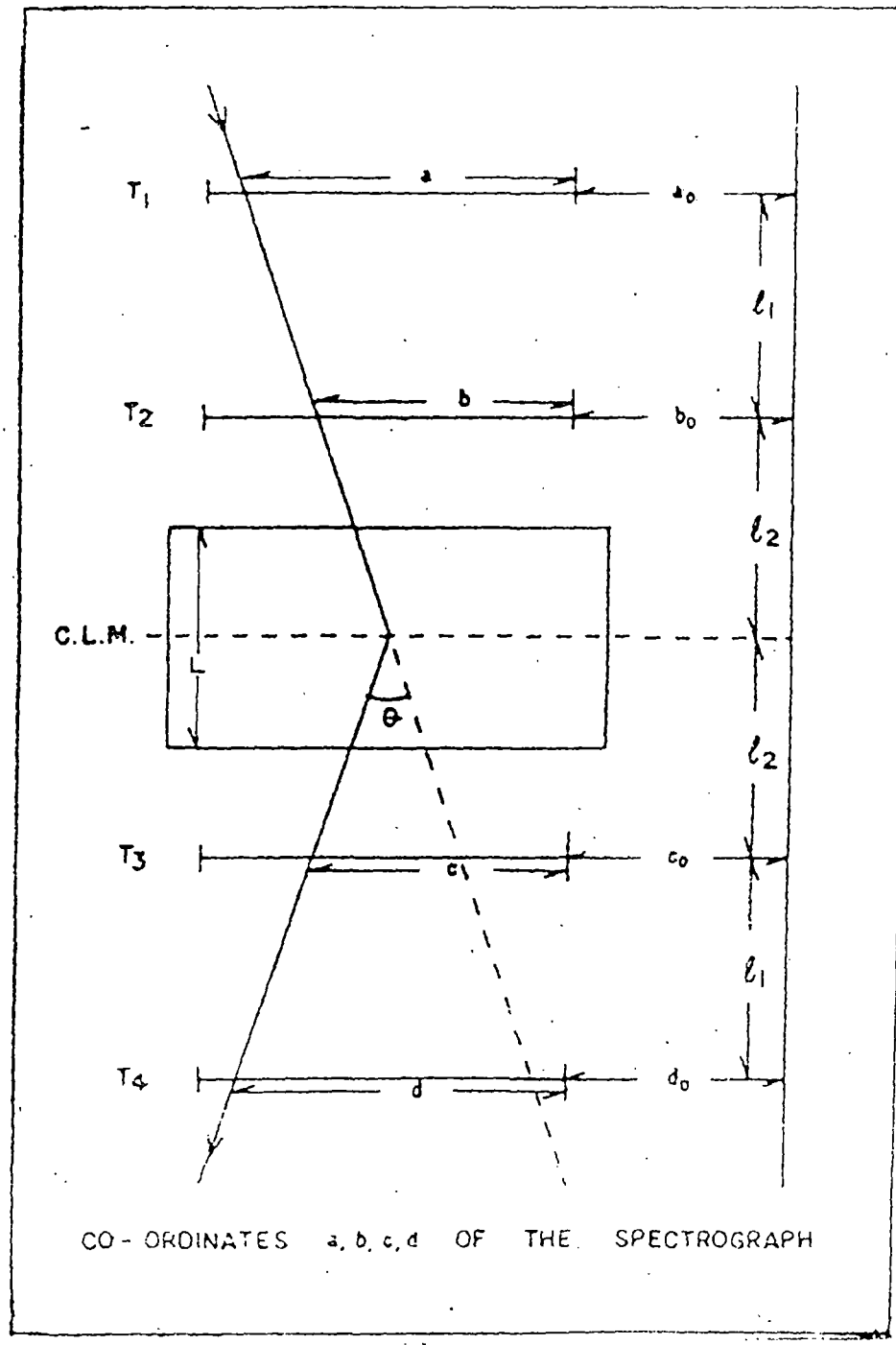

Fig. 3.18 THE COORDINATES a, b, c, d and a_0, b_0, c_0, d_0 FOR THE MAGNETIC SPECTROGRAPH SHOWN ALONG WITH THE MAGNET.

magnet) and the measurement of the geometrical constants of the spectrograph were done very carefully as they are of great importance for the measurement of the momentum of muons. Each flash-tube tray was fitted with two horizontal Perspex plates placed diagonally opposite and through each of which two very small holes of 1mm diameter were bored. The holes were in identical positions on each tray, calibrated by means of a cathetometer with an accuracy of 0.05mm. Four monofilament nylon threads (0.2-mm diameter) were passed through such holes situated at exactly identical positions at four corners of each tray. Each of these threads were tied to a brass (non-magnetic) bob at the bottom. Adjustment was made in such a way that each thread passed through all the four holes in the trays without touching the Perspex wall of 1mm bore. In this way all the flash tubes were made parallel to each other to an accuracy of 0.2 mm and the trays were bolted rigidly to the framework at correct position. The constants of the spectrograph indicated in the fig. 3.18, measured and previously reported by Sarkar [3], are given in Table- 3.2.

Table 3.2: The geometrical constants of the magnetic spectrograph.

Vertical dimension	**Distance in cm**	**Horizontal dimension**	**Relative distance in cm.**	
			Magnet 1 (M_1)	**Magnet 2 (M_2)**
l_1	85	a_o	0	0
l_2	85	b_o	-0.008	+0.010
		c_o	+0.006	- 0.009
L	105	d_o	-0.010	- 0.005
1 t.s. = 1.999 ± 0.002cm.				

SECTION-II

THE DATA ANALYSIS AND ERROR ESTIMATION

3.5 SCINTILLATION COUNTER DATA THE SHOWER PARAMETERS

In the present experiment, the shower parameters viz. the shower size (Ne), the core co-ordinates (X_0,Y_0) and the shower age (s) of air showers recorded by the array were determined by fitting the electron densities measured by the scintillation counters to the electron distribution function proposed by Hillas and Lapikens [11]. The choice of this particular function was encouraged by the results of an analysis performed by Bhattacharya et al. [12]. In this analysis, the authors had tested the data collected with NBU air shower array by studying their goodness of fit to different electron distribution functions proposed by Greisen [13], Capdeveille et al. [14] and Hillas & Lapikens [11]. Fitting the measured elctron densities to these functions they have reported of obtaining the mean values of the reduced χ^2 as 1.81, 1.80 and 1.77 respectively for the above three distribution functions.

Assuming any particular form of the function representing the distribution of electrons in the EAS, the four shower parameters (Ne, X_o&Y_o and s) can be calculated by using electron densities measured at four different points of the shower front. But, due to the possible existence of local fluctuation in densities, fluctuations arising due to the statistical nature of response of the detectors and random instrumental errors in the measurement of the densities, statistical fitting of the observed experimental data is usually performed to estimate the shower parameters. The statistical method used in the present experiment, reported previously by Basak and Chaudhuri [2], was the most widely used method of χ^2-minimisation by steepest descent. The process involved in it is an iterative process for determining the required parameters by adjusting the values of the parameters such that the value of χ^2 defined as,

$$\chi^2 = \sum_{i=1}^{n} W_i \left(\Delta_{o,i} - \Delta_{e,i} \right)^2$$

is minimum. Here, $\Delta_{o,i}$ and $\Delta_{e,i}$ are the densities observed and expected at the i-th detector respectively. W_i is the weightage factor attached with each measurement of the predicted densities and n is the number of detectors.

In principle, it is possible to obtain the best fit values for the four variables X_o,Y_o, s and Ne by solving four simultaneous equations of the form,

$$\partial\chi^2 / \partial\xi_i = 0$$

where, ξ_i represents the above four variables. However, these equations being highly non-linear, an iterative procedure was used for minimizing χ^2 using the method of steepest descent. To start this iterative procedure the initial estimates of these parameters are necessary. The initial estimates of the core location were made by using the symmetry of the lateral distribution function. The 'centre of gravity' of the density distribution is given by,

$$X_o = \sum_{i=1}^{n} \Delta_{o,i} X_i / \sum_{i=1}^{n} \Delta_{o,i}$$
$$Y_o = \sum_{i=1}^{n} \Delta_{o,i} Y_i / \sum_{i=1}^{n} \Delta_{o,i}$$

where X_i, Y_i are the coordinates of the i-th detector. The correction to consider the inclination of incident shower to the plane of detectors was ignored, as the angular distribution of showers is rather steep. An initial estimate of s was obtained from the logarithmic slope of the density distribution around the density weighted center. Then, given a set of values for X_o, Y_o and s, the corresponding value of Ne was obtained by solving the equation,

$$\partial\chi^2 / \partial Ne = 0.$$

which gives a cubic equation of type ,

$$Ne^3 + C\,Ne + t = 0$$

where C and t are the functions of core location and age (s).

With these initial estimates of X_o, Y_o, s and Ne, the values of χ^2 and the various components of $\nabla\chi^2$ were calculated. The wieghtage factor W_i was taken to be $W_i = 1 / \Delta_{e,i}^2$.

The quantity χ^2 can be taken to be representing a surface in 4-dimensional space (X_o, Y_o, s and Ne) . The air shower parameters were obtained by locating the minimum of that surface. With the calculated values of χ^2 and $\nabla\chi^2$ the initial estimates of the X_o, Y_o and s were incremented by an amount proportional to the respective component of $\nabla\chi^2$ in the direction of $-\nabla\chi^2$. With these new X_o, Y_o and s the new χ^2 and $\nabla\chi^2$ were calculated. These new values were accepted if the new χ^2 was less than the old. If the new χ^2 was greater than the old χ^2 , the new values were rejected and the increments were scaled down by a factor of two and the process was continued until the difference between the successive χ^2 per degree of freedom was less than 0.01 and the current values of X_o, Y_o, s and Ne were taken as the best fit values of the shower parameters. It was observed from the analysis of artificially

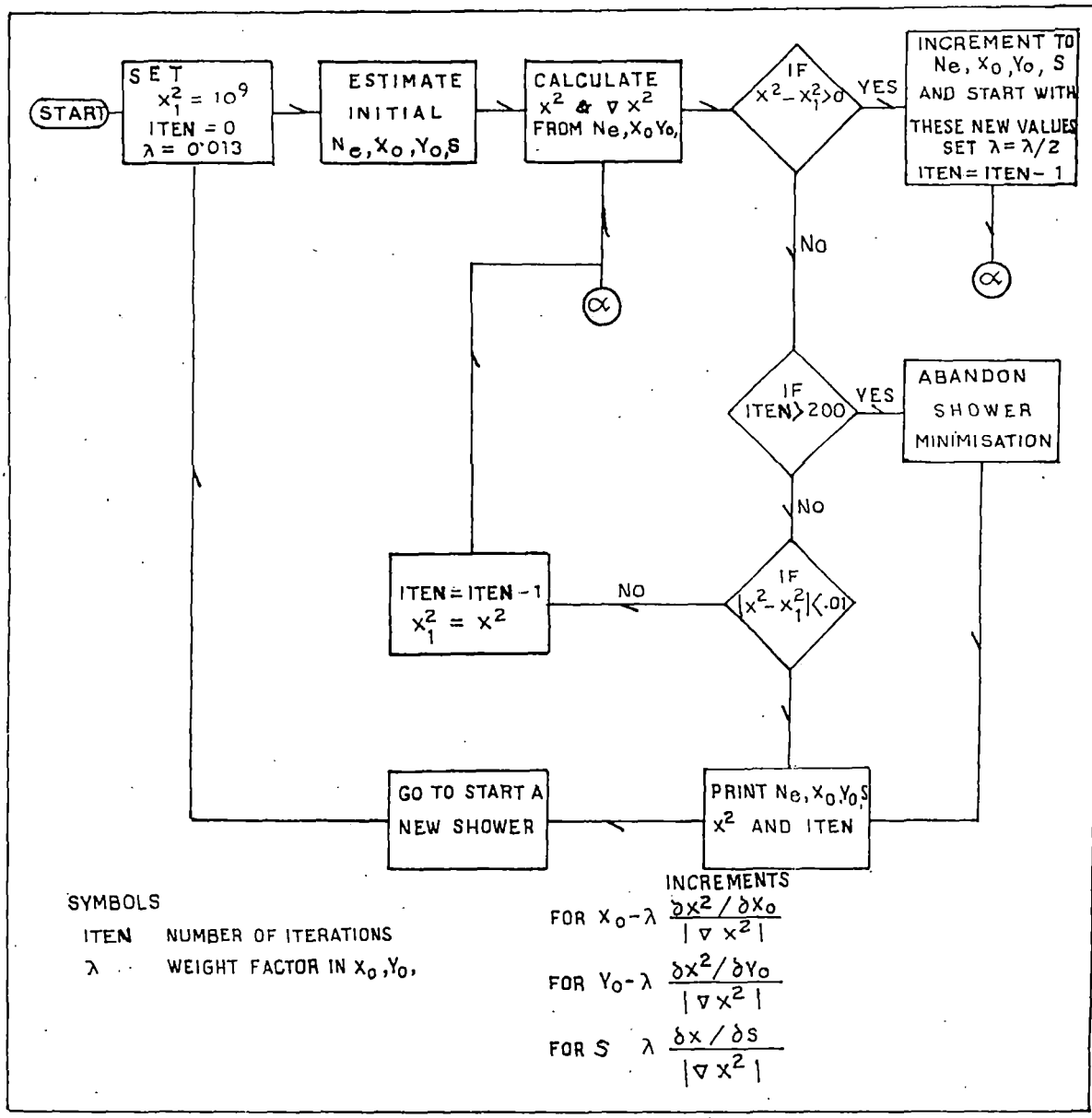

Fig. 3·19. A simple flow chart for x^2 minimisation procedure used for the analysis of AIR SHOWER DATA .

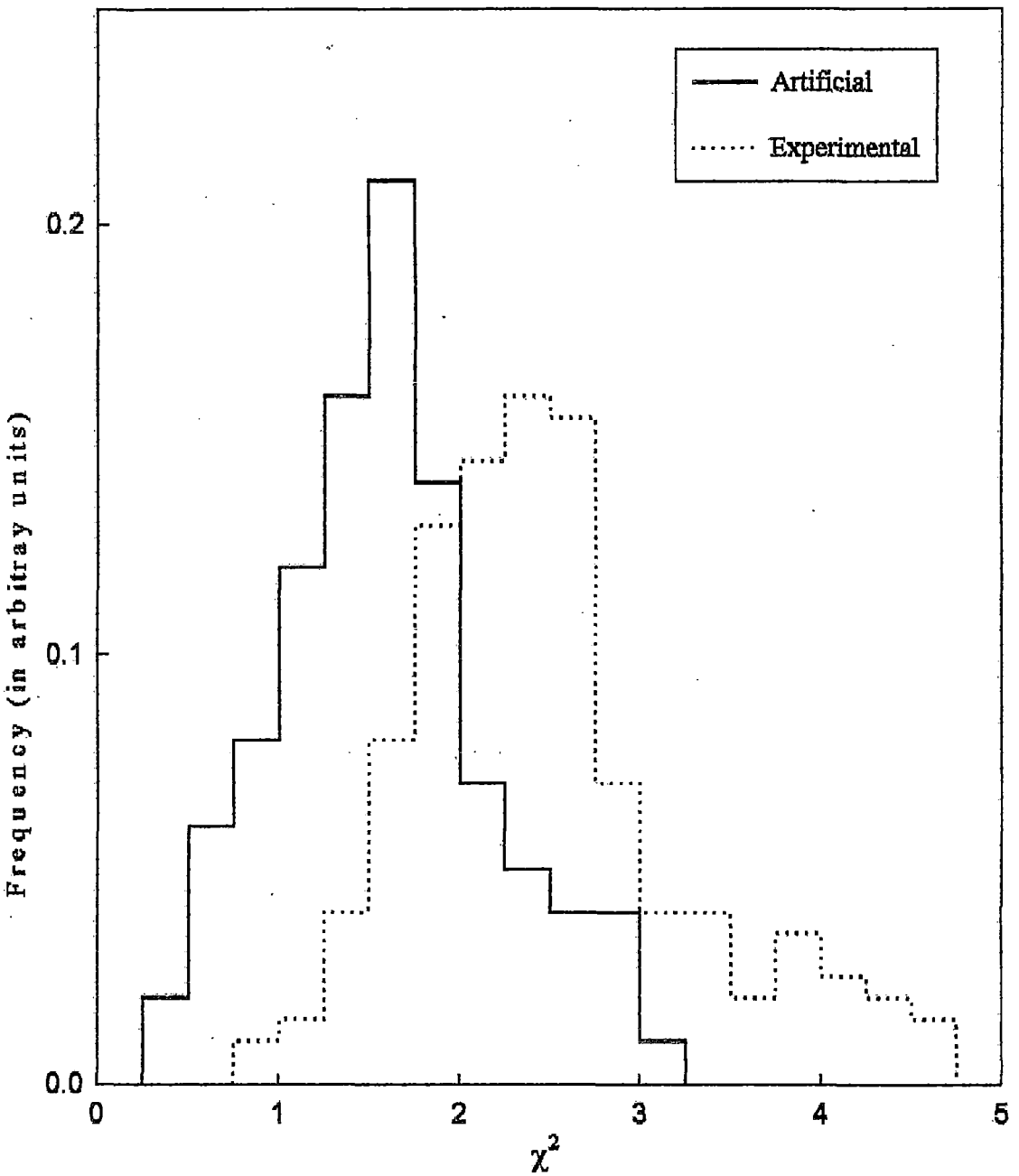

Fig.3.20(a) DISTRIBUTION OF REDUCED χ^2 FOR ARTIFICIALLY SIMULATED AND EXPERIMENTALLY OBSERVED AIR SHOWERS OF AVERAGE SIZE- 2 X 10^4.

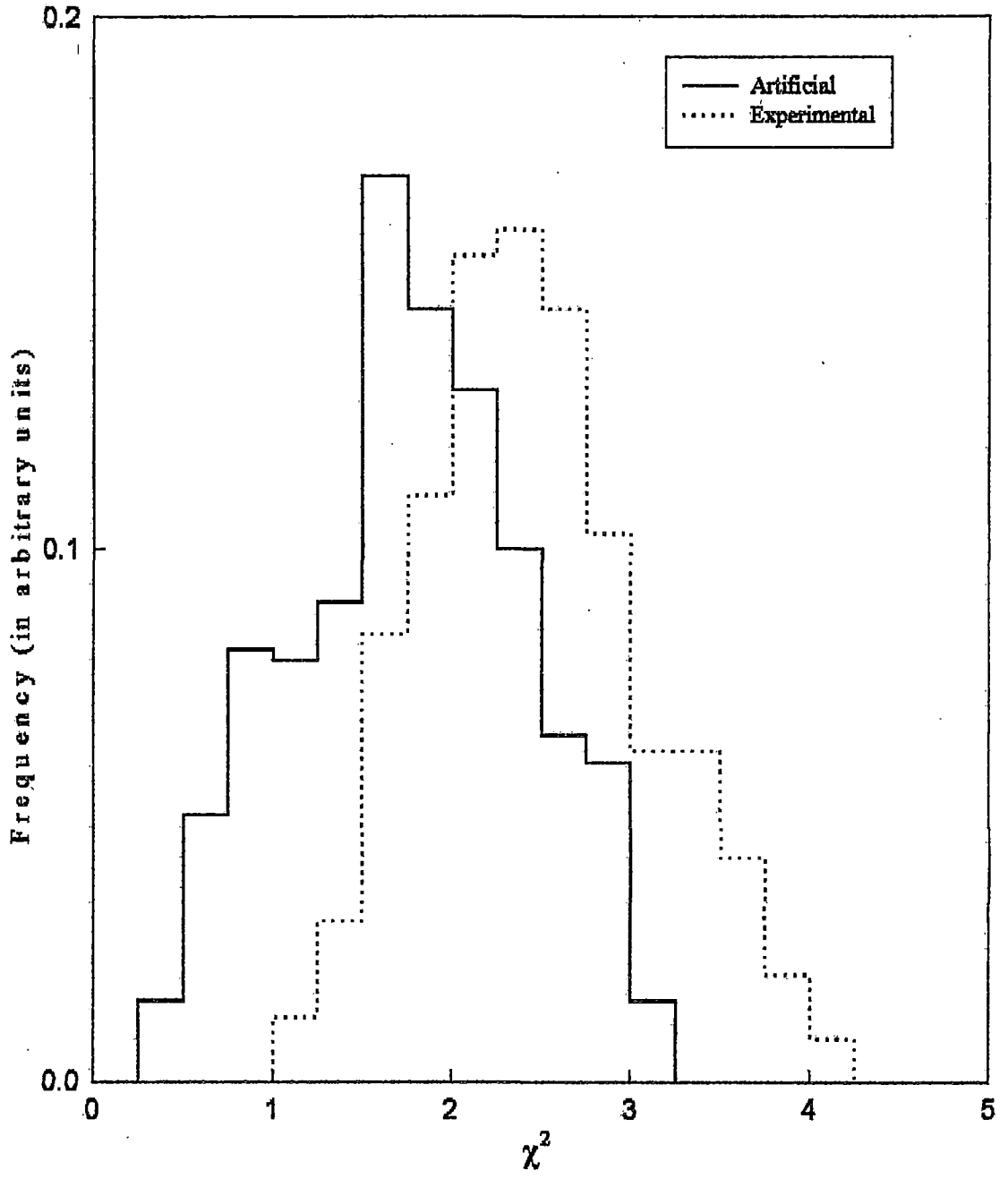

Fig.3.20(b) DISTRIBUTION OF REDUCED χ^2 FOR ARTIFICIALLY SIMULATED AND EXPERIMENTALLY OBSERVED AIR SHOWERS OF AVERAGE SIZE- 10^5.

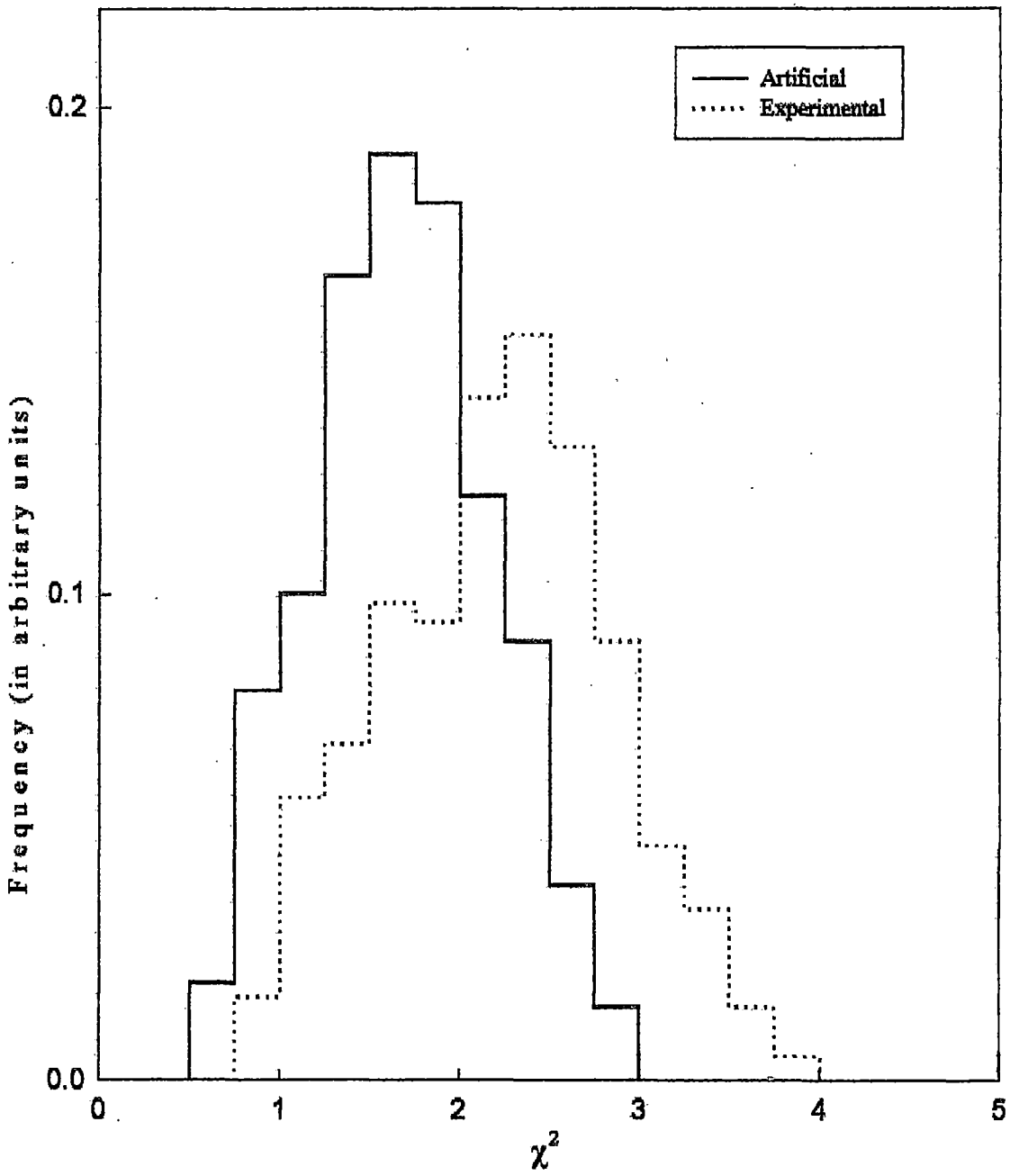

Fig.3.20(c) DISTRIBUTION OF REDUCED χ^2 FOR ARTIFICIALLY SIMULATED AND EXPERIMENTALLY OBSERVED AIR SHOWERS OF AVERAGE SIZE- 10^6.

simulated showers that the above condition ensured the final χ^2, to be very close to the minimum. If the above condition was not reached within 500 iterations, the further minimization was abandoned and the current values of the parameters were accepted, since in such cases it was observed that the values oscillate between two values very close to the minimum.

A flow chart for χ^2-minimisation procedure for finding the shower parameters is shown in fig. 3.19. A regular check on the analysis was kept by plotting the distribution of reduced χ^2 for each set of shower analyzed. A typical distribution of reduced χ^2 is shown in fig. 3.20(a) to 3.20(c).

3.6 MAGNETIC SPECTROGRAPH DATA : THE MOMENTUM OF MUONS

The muons associated with the air showers were detected and their momentum were measured by the magnetic spectrographs of the air shower array by measuring the deflections suffered by them while passing through the magnetic field. The method of calculation of muon momentum and the maximum detectable momentum (m.d.m.) of the spectrographs was earlier reported by Basak et al [15].

The momentum p of a particle with charge e, is related to the radius of curvature ρ of its path through a magnetic field B by the equation,

$$p = 300\ B\ \rho\ eV/c \quad .... \quad ..... \quad ..... \quad (3.1)$$

If dl be the element of path normal to the field then the radius of curvature ρ can be written as,

$$\rho = \frac{dl}{d\theta}$$

Here θ is the deflection suffered by the particle due to the magnetic field in radians. Combining these two, we get

$$\theta = 300 \int (B\ dl) / p$$

Neglecting the energy loss in the material, the momentum p(eV/c) is given by,

$$p = (300 \int B\ dl) / \theta \qquad (3.2)$$

where, B is in gauss and l is in cm.

In the magnetic spectrographs of the NBU array, the angular deflection θ of the muons can be calculated from the coordinates of the muon track located by the flashes of neon flash-tubes arranged in 4 trays (T_1, T_2, T_3 and T_4). The coordinates are illustrated in fig.3.18. The relationship between these coordinates and the angular

deflection, considering the small angle approximation, can be shown to be as,

$$\theta = \frac{1}{l_2}[(b-a) + (c-d) + (b_o-a_o) + (c_o-d_o) \qquad (3.3)$$

for the muons traversing all four trays. If the muon traverses only upper three trays out of the four then θ is given by,

$$\theta = \frac{1}{l_2}\ [\ 2(b-a) - (c-b) + 2(b_o-a_o) - (c_o-b_o)\ ] \qquad (3.3a)$$

and if it traverses the lower three trays then

$$\theta = \frac{1}{l_2}\ [\ (c-b) - 2(d-c) + (c_o-b_o) - 2(d_o-c_o)\ ] \qquad (3.3b)$$

Therefore, writing the deflection in general as $\theta = \frac{\delta}{l_2}$, the momentum of the muon can be written from equation 3.2 as,

$$p = \frac{l_2}{\delta}[300\ .B.L] = \frac{C}{\delta} \qquad (3.4)$$

Thus the momentum p is related to the quantity δ, which is directly determined from the coordinates a, b, c and d. For NBU magnetic spectrographs B = 16.2 K.Gauss with the operating current of 15 amps, L the effective magnetic length = 100 cm. So the value of C is 20.67 GeV /c (t.s.).

3.6.1 Determination of the Momentum

As explained above the momentum of the muons recorded by the magnetic spectrographs can be determined by finding the value of the quantity δ, which is related to the co-ordinates of the muon trajectory by the equation 3.3. And, the co-ordinates of the muon trajectories are measured from the photographic records of the spectrograph

The flashes of the tubes those are discharged by the passage of muons represent the trajectory of the muons and are recorded in photographic films. The exact position of the tubes flashed in the trays are determined by projecting these films on a vertical board by a 35 mm film projector. These boards contain the serial number of the tubes with respect to the fiducial marks, which serves as the reference marks. So, with these fiducial marks as the reference, images of the flashed tubes are positioned on these boards and the row and column numbers of the tubes from each tray are recorded on a data sheet. Then a scale diagram of a portion of flash-tube tray, which is enlarged by a factor of 2.5 in the horizontal direction and by a factor of 0.54 in the vertical direction (shown in fig. 3.21), is taken and a cursor is adjusted on this

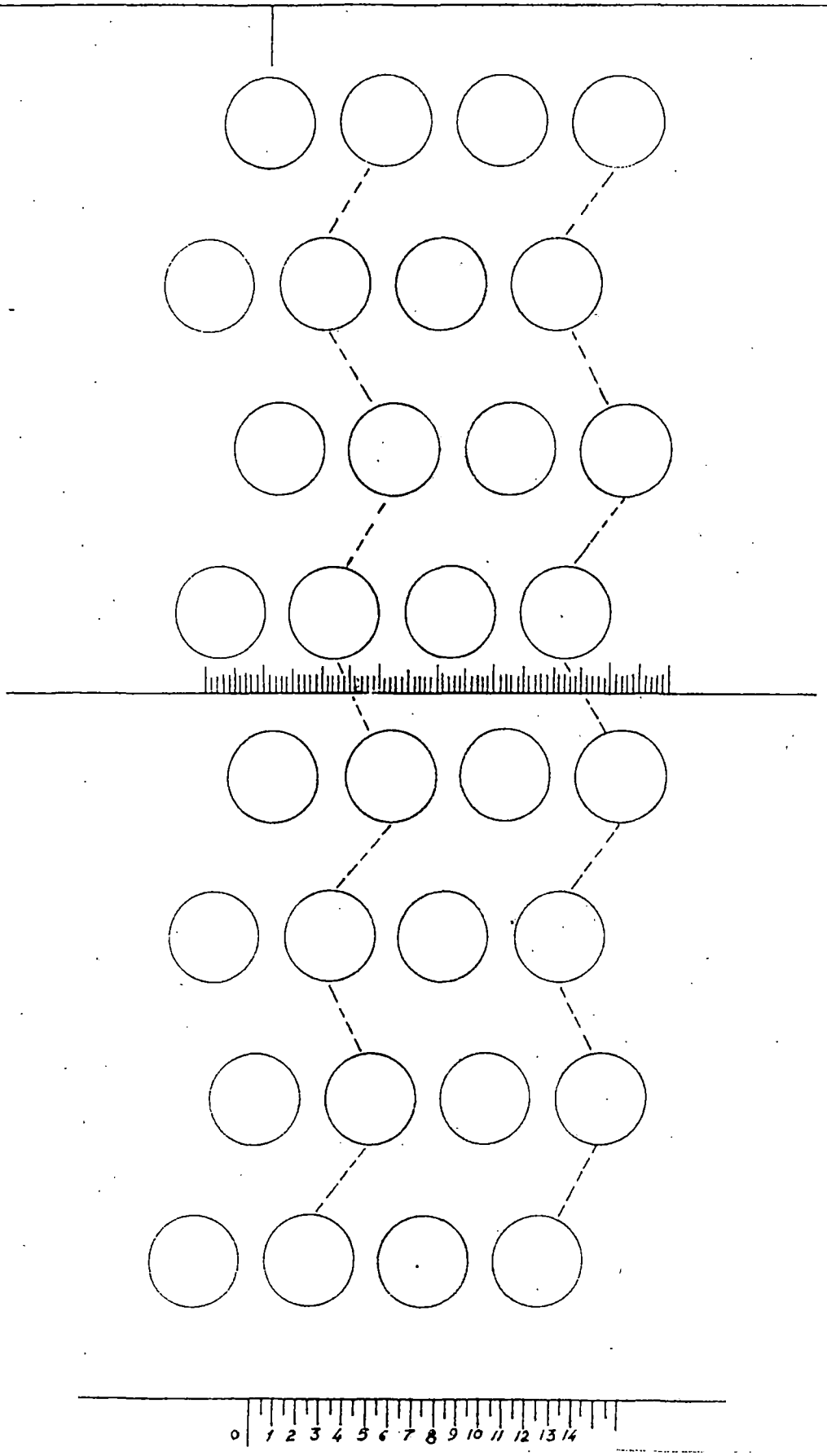

Fig. 3.21 SCALE DIAGRAM OF A PORTION OF FLASH TUBE TRAY.

diagram according to the row and column numbers of the flashed tubes as recorded on the data sheet mentioned above. The intersection of the cursor and the scale in diagram gives the co-ordinate of the trajectory. The mean value of the coordinates of the two extreme limits of the track is recorded. It might be mentioned here that this method of analysis called the track simulation method was developed by Hyman and Wolfendale (16) and has been proved quite accurate for high- energy particles.

3.6.2 MAXIMUM DETECTABLE MOMENTUM OF THE MAGNETIC SPECTROGRAPH

The momentum which corresponds to the deflection equal to the most probable error in the deflection measurement is referred as the maximum detectable momentum (m.d.m.) of the magnetic spectrograph. If the spectrograph is exactly symmetrical about the central line and provided there is no other cause of deflection except the magnetic field, then the trajectory of the particle will be as shown in fig.3.18. The incident and emergent path will meet at a single point on the central line of the magnet (C.L.M.). However, due to different reasons slight deviations between these two paths are observed. The possible reasons of this discrepancy, represented by ε, can be mainly,

(i) the finite diameter of the neon flash-tubes causing an error while locating the muon track.

(ii) multiple coulomb scattering of muons and

(iii) loss of energy by the muons while traversing through the magnet, particularly for low energy particles

This quantity ε determines the accuracy with which measurement of the deflection and hence the momentum is possible by the spectrograph. Referring to fig. 3.18, ε can be written as,

$$\varepsilon = X_{ab} - X_{cd} \quad \ldots \quad \ldots \quad \ldots (3.5)$$

where

$$X_{ab} = b - \frac{l_2}{l_1}(a - b) + b_o - \frac{l_2}{l_1}(a_o - b_o)$$

and

$$X_{cd} = c - \frac{l_2}{l_1}(d - c) + c_o - \frac{l_2}{l_1}(d_o - c_o)$$

Furthermore, considering the contribution to ε from the later two reasons listed above to be small, the only contribution to ε can be attributed to the first reason or the track location error. And, assuming the existence of equal amount of errors σ_i

in location of track in all the four trays of flash tubes, the standard error in measurement of deflection or the quantity δ can be written as,

$$\sigma_\delta = 2\,\sigma_i \qquad \ldots\ldots \qquad \ldots\ldots \qquad \ldots\ldots \qquad (3.6)$$

Similarly the error in determining ε from equation (3.5) will be,

$$\sigma_\varepsilon = \sqrt{2}\,\sigma_i\,[\,(1+\,l_2/l_1)^2 + (\,l_2/l_1\,)^2\,]^{1/2}$$

Using the measured values of l_2 and l_1 from the Table- 3.1,

$$\sigma_\varepsilon = \sqrt{10}\,\sigma_i$$

$$\text{or,} \quad \sigma_i = \frac{\sigma_\varepsilon}{\sqrt{10}}$$

Putting this in equation we get the error in δ as,

$$\sigma_\delta = \frac{2}{\sqrt{10}}\sigma_\varepsilon \qquad \ldots\ldots \qquad \ldots\ldots \qquad (3.7)$$

So, the m.d.m. of the spectrograph, defined as the momentum corresponding to the deflection equal to the most probable error on the measured deflection, is given by the equation 3.4 as,

$$\text{m.d.m.} = \frac{C}{0.6745\,\sigma_\delta} = \frac{C}{0.6745\,\sigma_\varepsilon} \qquad \ldots\ldots \qquad (3.8)$$

And, the value of m.d.m. of magnetic spectrograph of NBU array corresponding to $\sigma_\varepsilon = 0.100(\pm 0.005)$, measured previously and reported by Sarkar [3], is equal to 484(±23) GeV/c.

3.6.3 Measurements with Zero Magnetic Field

To check the alignment of the spectrograph, it was operated by G.M. coincidence only without passing any current through the coils of the magnet and keeping the systems controlling the array of scintillation counters off. 580 particles were recorded in about 16 hours of this operation. The observed frequency distribution of the deflections of recorded muons is shown in fig. 3.22. In this condition the observed deflections are due to the errors in location of tracks at each tray and the multiple Coulomb scattering in the iron. The distribution was compared with the Gaussian distribution (continuous curve in the figure) with the same standard deviation. Since both the above mentioned effects cause the deflections positive and negative with equal probability and hence shows the Gaussian distribution with a mean value zero. The obtained sharp Gaussian curve means, the error in alignment of the trays was quite small.

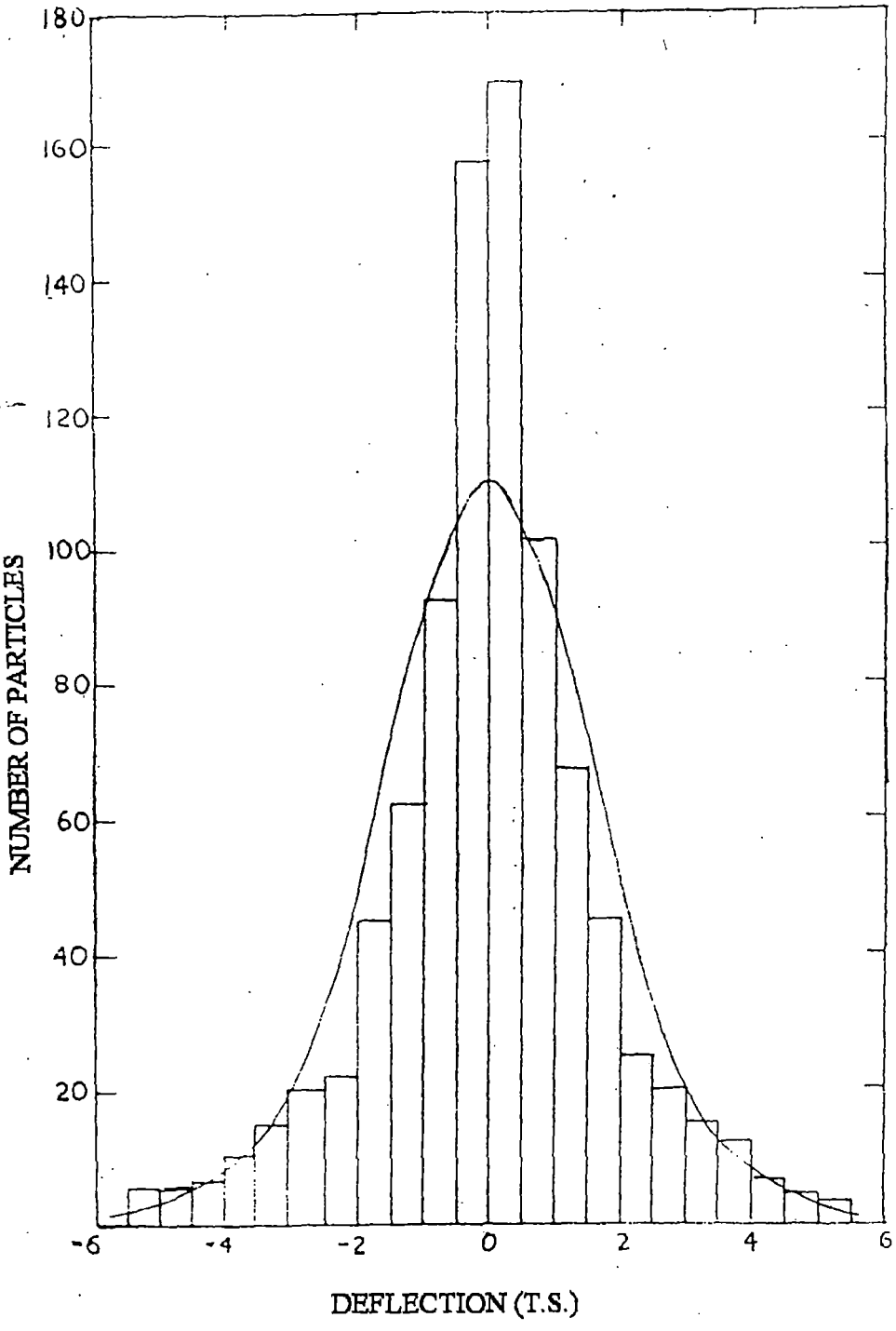

Fig. 3.22 THE ZERO FIELD DISTRIBUTION OF δ.

3.7 SIMULATION OF ARTIFICIAL AIR SHOWERS

Simulating air shower events artificially with the help of a particular lateral distribution function describing the distribution of electrons and analysing the calculated data representing the simulated events with the method applied for the analysis of actual experimental measurements serves two purposes. First, it gives an estimate of the errors in determination of different shower parameters, which are obtained by fitting experimentally measured electron densities to the chosen distribution function. Secondly, from this analysis the detection efficiency of the array can also be investigated.

In the present experiment, to simulate artificial air shower events, the array was divided into different annular rings around the center of the array, for computational convenience, and some particular values of shower size and age were chosen. Then, selecting the position of the shower core randomly within a particular annular ring the densities expected at each of the scintillation detectors were calculated using the lateral distribution function proposed by Hillas and Lapikens [11]. Poissonian fluctuations were superposed to these calculated densities, to make them similar to those recorded by the detectors in the experiment. These densities were than utilized to estimate the errors in the determination of shower parameters and detection efficiency of the array. In the present experiment 500 such showers were generated in each annular ring for a given shower size and age, and the process was repeated by varying the shower size.

3.7.1 ERROR IN SHOWER PARAMETERS

The electron densities of the artificial showers obtained in the above manner were fitted to the same lateral distribution function to calculate the shower parameters by the same method of χ^2-minimisation that was utilized to analyse the measurements of the experiment. The deviations of these calculated shower parameters with those originally chosen gave an estimate of the errors that could be present in the calculations of the EAS parameters from the measured electron densities in the experiment. A few sample histogram plots of the frequencies of observed deviations are shown in the fig. 3.23 & 3.24. The average values of the errors or the uncertainties in determination of shower size, age and core positions were estimated to be ± 0.15Ne, ± 0.09 and ± 1.1 meter respectively.

3.7.2 THE DETECTION EFFICIENCY OF THE ARRAY

The fraction of the number of showers those are detected by the array out of the total number of showers incident over it is referred as the detection efficiency of the array. Generally it is expected that if the coincidence and triggering conditions of the array are satisfied by the incident air shower the shower event should be recorded by the array. However, due to statistical fluctuation in densities, the detection efficiency of individual detectors and some systematic errors the shower detection efficiency of the array is usually seen to be a function of the distance from the center of the array.

To study the variation of the detection efficiency with the distance from the centre of the array for showers of different sizes, the showers generated artificially in the above mentioned manner were utilised. The artificially simulated showers with core locations at different positions were checked according the selection criteria and the percentage of the showers selected from the total showers were calculated. The observed variation of efficiency with the radial distance for the showers of two different sizes are shown in fig. 3.25.

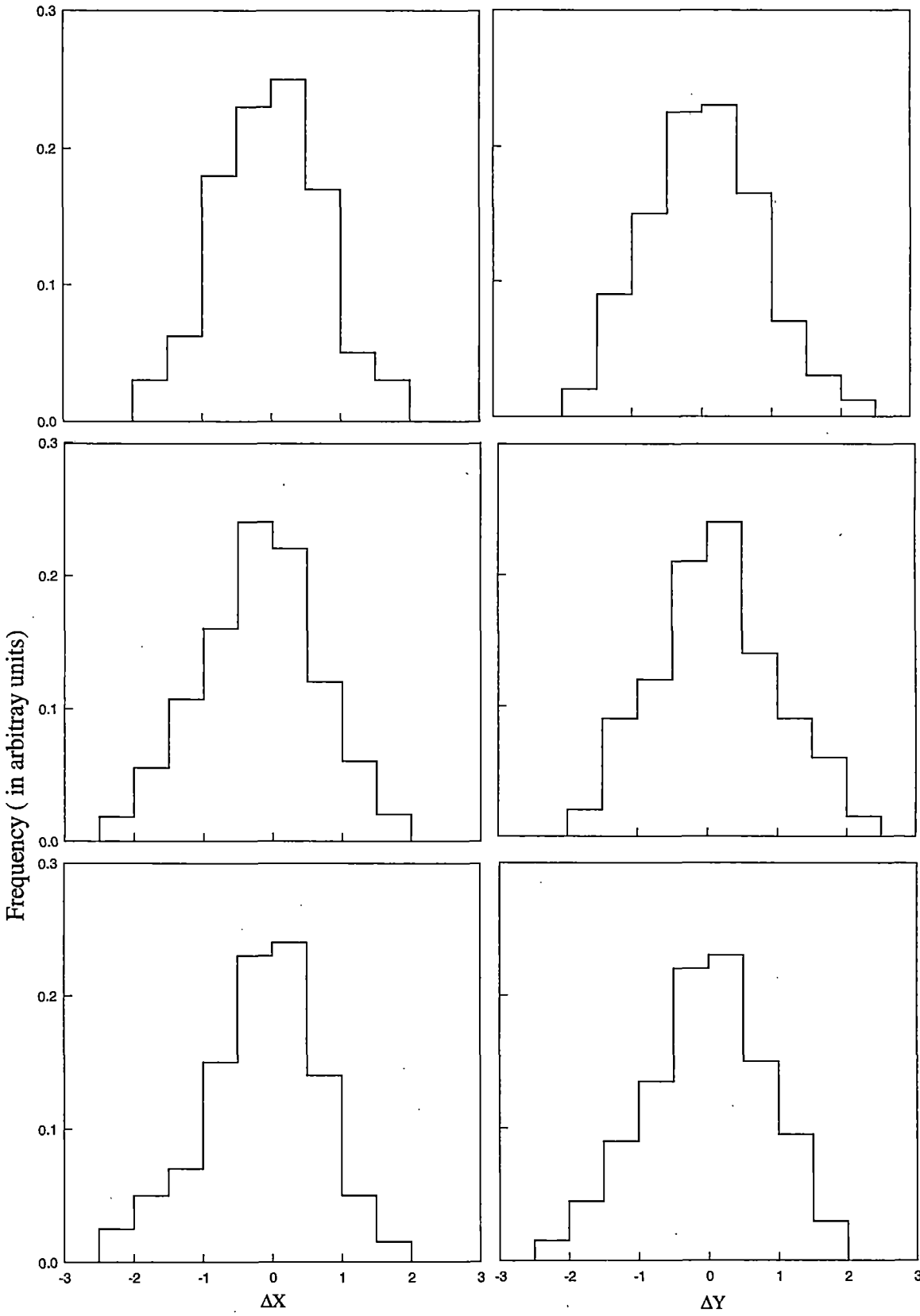

Fig. 3.23 THE DISTRIBUTION OF ERRORS IN ESTIMATION OF CO-ORDINATES (X_0&Y
OF THE SHOWER CORE OBTAINED FROM THE ANALYSIS OF ARTIFICIAL
AIR SHOWERS SIMULATED WITH THE INITIAL VALUES OF AGE (S)=1.2 AN
SIZE (Ne) = 2.10^4 (TOP), 10^5 (MIDDLE) AND 10^6 (BOTTOM).

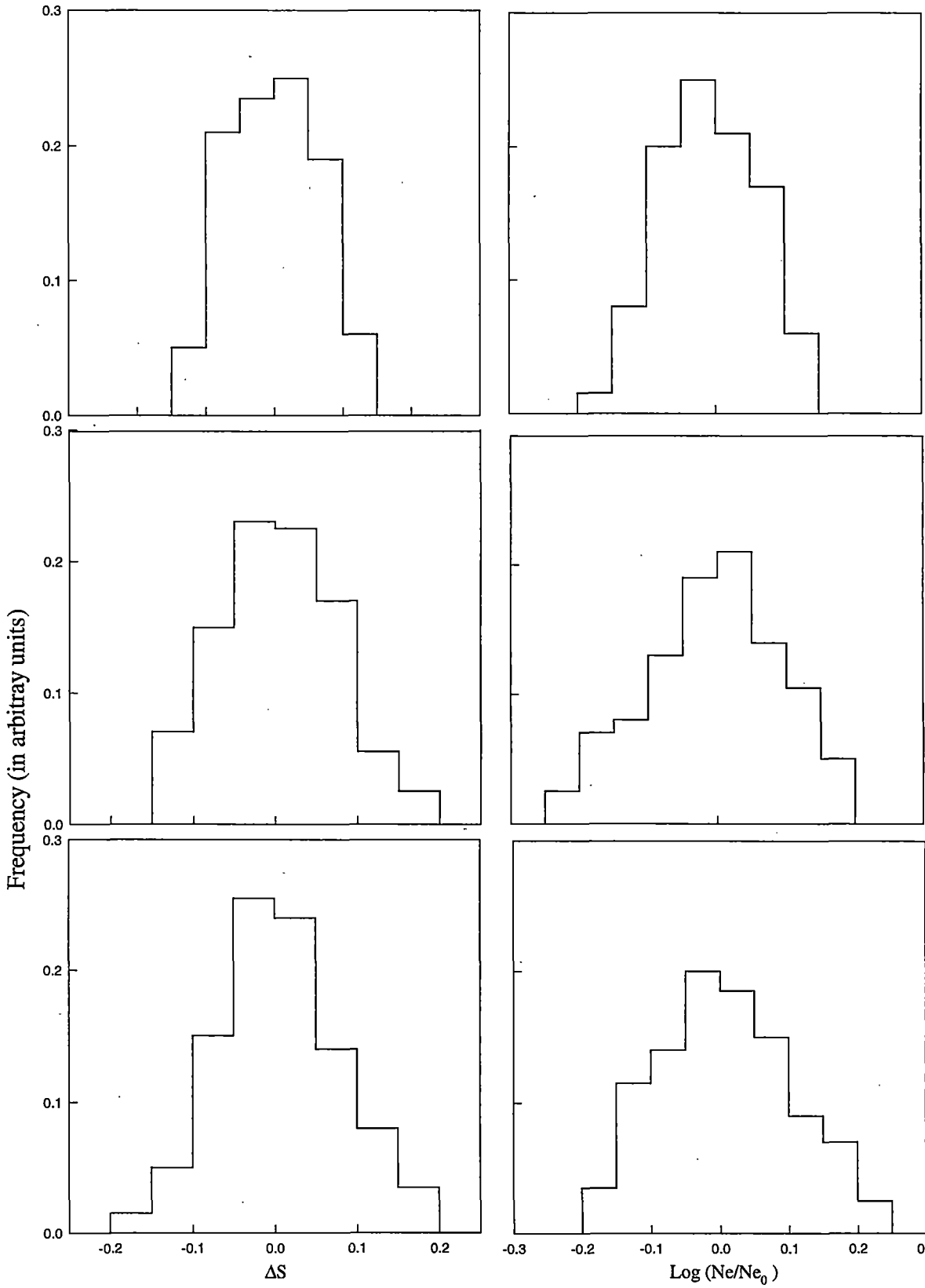

Fig. 3.24 THE DISTRIBUTION OF ERRORS IN ESTIMATION OF SHOWER AGE (S) AND SIZE (Ne) OBTAINED FROM THE ANALYSIS OF ARTIFICIAL AIR SHOWERS SIMULATED WITH THE INITIAL VALUES OF AGE (S) = 1.2 AND SIZE (Ne) = 2.10^4(TOP), 10^5 (MIDDLE) AND 10^6 (BOTTOM).

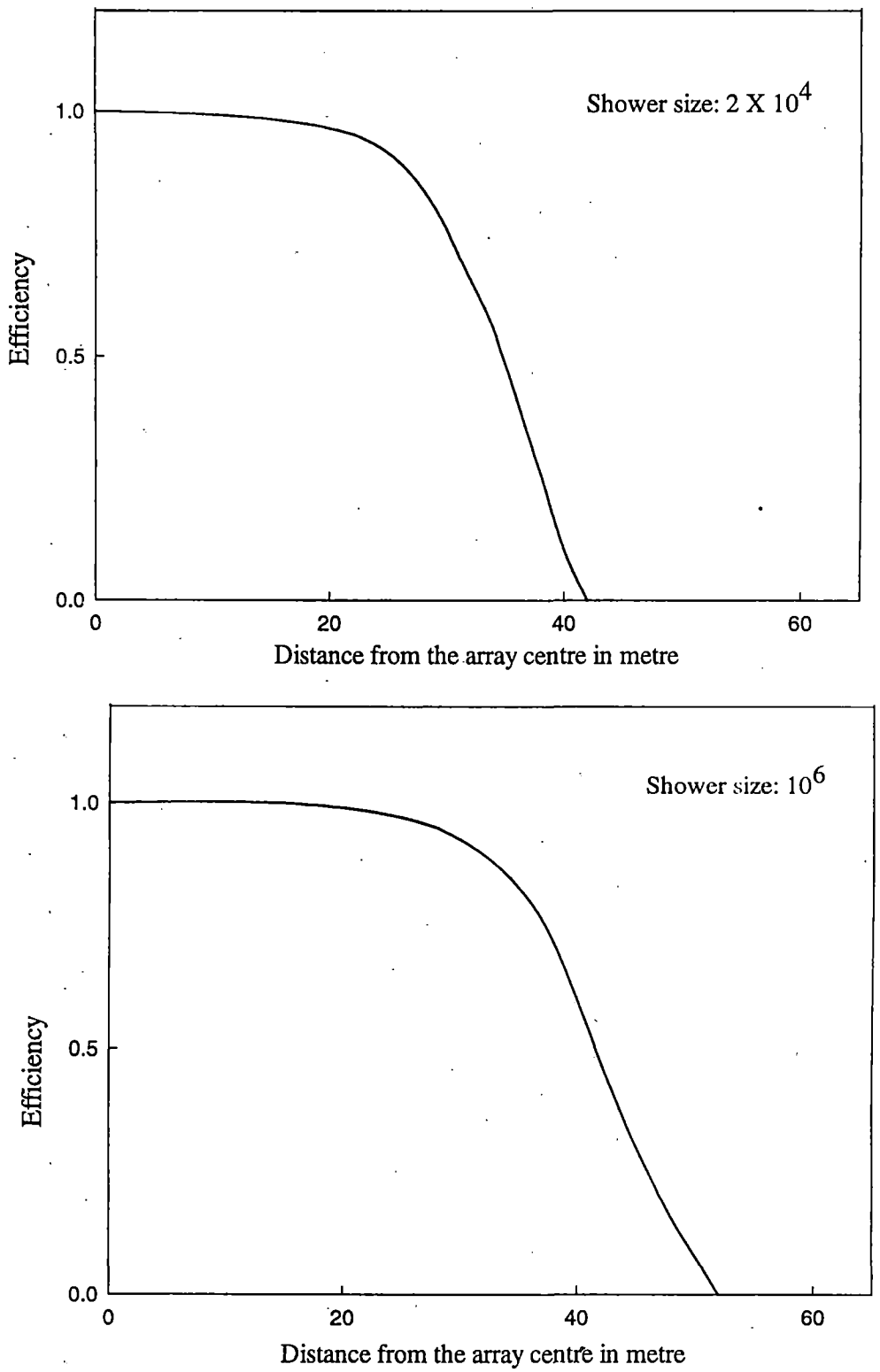

Fig. 3.25 VARIATION OF DETECTION EFFICIENCY OF THE ARRAY WITH DISTANCE FROM THE ARRAY CENTRE FOR AIR SHOWERS OF TWO DIFFERENT SIZES.

REFERENCES

1 D. K. Basak, N. Chakraborty, B. Ghosh, G. C. Goswami and N. Chaudhuri, *Nucl. Inst. Meth.*, **227**(1984), 167

2 D. K. Basak and N. Chaudhuri, *Nuovo Cimento*, **C9** (1986), 846

3 S. K. Sarkar, *Ph.D. Thesis (1987),* North Bengal University, India.

4 G. C. Goswami, B. Ghosh, M. R. Ghoshdastidar and N. Chaudhuri, *Nucl. Inst. Meth.*, **199** (1982), 505

5 M. Conversi and A. Gozzini, *Nuovo Cimento*, **2** (1955), 189.

6 G. Barsanti, M. Conversi, S. Focardi, G. P. Murtas, C. Rubbia and G. Torelli, *Proc. CERN Symp.*, **2** (1956), 56.

7 M. Gardener, S. Kisdnasamy, E. Rossle and A. W. Wolfendale, *Proc. Phys. Soc.*, **B70** (1957), 687.

8 H. Coxell and A. W. Wolfendale, *Proc. Phys. Soc.*, **75** (1960), 378.

9 H. Coxell, *Ph.D. Thesis* (1961), University of Durham, London.

10 G. C. Goswami, B. Ghosh, M. R. Ghoshdastidar, S. K. Sengupta and N. Chaudhuri, *Nucl. Insts. Meths*, **192** (1982), 375.

11 A. M. Hillas and J. Lapikens, *15th ICRC* (Plovdiv, 1977), **8,** 460.

12 B. Bhattacharya, A. Bhadra, A. Mukherjee, G. Saha, S. Sanyal, S. Sarkar, B. Ghosh and N. Chaudhuri, *IL Nuovo Cimento*, **18C** (1995), 325.

13 K. Greisen, *Ann. Rev. Nucl. Sci.*, **10** (1960), 63.

14 J. N. Capdevielle, J. Gawin, J. Procureur, *15th ICRC* (Plovdiv, 1977), **8**, 341.

15 D. K. Basak, N. Chaudhuri, S. Sarkar, B. Bhattacharya and B. Ghosh, *Nuovo Cimento*, **10C** (1987), 169

16 P. J. Hyman and A. W. Wolfendale, *Proc.Phy.Soc.*, **80** (1962), 710